Since January 2020 Elsevier has created a COVID-19 resource centre with free information in English and Mandarin on the novel coronavirus COVID-19. The COVID-19 resource centre is hosted on Elsevier Connect, the company's public news and information website.

Elsevier hereby grants permission to make all its COVID-19-related research that is available on the COVID-19 resource centre - including this research content - immediately available in PubMed Central and other publicly funded repositories, such as the WHO COVID database with rights for unrestricted research re-use and analyses in any form or by any means with acknowledgement of the original source. These permissions are granted for free by Elsevier for as long as the COVID-19 resource centre remains active.

Nano Energy 79 (2021) 105369

Contents lists available at ScienceDirect

Nano Energy

journal homepage: http://www.elsevier.com/locate/nanoen

Recent advances in energy-saving chemiresistive gas sensors: A review

Sanjit Manohar Majhi [a,b,1], Ali Mirzaei [c,1], Hyoun Woo Kim [a,b,**], Sang Sub Kim [d,***], Tae Whan Kim [e,*]

[a] Division of Materials Science and Engineering, Hanyang University, Seoul, 04763, South Korea
[b] The Research Institute of Industrial Science, Hanyang University, Seoul, 04763, South Korea
[c] Department of Materials Science and Engineering, Shiraz University of Technology, Shiraz, 715557-13876, Iran
[d] Department of Materials Science and Engineering, Inha University, Incheon, 22212, South Korea
[e] Department of Electronics and Computer Engineering, Hanyang University, Seoul, 04763, South Korea

ARTICLE INFO

Keywords:
Energy saving
Low-power consumption
Room-temperature sensing
MEMS-Based gas sensors
Flexible gas sensors

ABSTRACT

With the tremendous advances in technology, gas-sensing devices are being popularly used in many distinct areas, including indoor environments, industries, aviation, and detectors for various toxic domestic gases and vapors. Even though the most popular type of gas sensor, namely, resistive-based gas sensors, have many advantages over other types of gas sensors, their high working temperatures lead to high energy consumption, thereby limiting their practical applications, especially in mobile and portable devices. As possible ways to deal with the high-power consumption of resistance-based sensors, different strategies such as self-heating, MEMS technology, and room-temperature operation using especial morphologies, have been introduced in recent years. In this review, we discuss different types of energy-saving chemisresitive gas sensors including self-heated gas sensors, MEMS based gas sensors, room temperature operated flexible/wearable sensor and their application in the fields of environmental monitoring. At the end, the review will be concluded by providing a summary, challenges, recent trends, and future perspectives.

1. Introduction

Due to rapid industrialization and urbanization, the world is facing the problem of severe air pollution, as witnessed by the increasingly large amounts of deleterious and pollutant gases being introduced into the environment. To name a few, these pollutants consist of several toxic gases such as CO, SO_2, NO_2 and H_2S and/or chemicals and volatile organic compounds (VOCs) such as benzene, toluene, ethanol, acetaldehyde and formaldehyde. The presence of toxic gases and VOCs can be detrimental to humans and the surrounding atmosphere [1–3]. For instance, an estimated 3.8 million people per year face severe illnesses that may prove fatal and can be attributed to air pollution. Moreover, near 20% of cardiovascular deaths and about 20% of deaths due to stroke can be attributed to household pollution [4]. Moreover, toxic gases can significantly affect the respiratory tract and may even be harmful to the nervous and the immune systems [5,6]. In particular, severe air pollution can cause abnormalities in lung surfactant composition and damage to the lungs, making humans more vulnerable to diseases such as COVID-19 [7]. Accordingly, air pollution has become a pressing global problem, prompting several health agencies to recommend short-time exposure limits (STELs) for various toxic and VOC gases [8,9]. Moreover, if the potential risk to human health is to be reduced, pollutant gases in the air must be continuously monitored using sensitive and reliable electronic devices.

Nowadays, the detection of dangerous gases is becoming increasingly important in different industries, indoor and outdoor air quality monitoring, public safety, mines, and so on [8–11], As a result, numerous sensing techniques, such as the electrochemical [12], optical fiber [13], quartz crystal microbalance (QCM) [14] and capacitive [15] techniques, have been applied for this purpose. However, most of these techniques have disadvantages such as relatively high price, low sensitivity and selectivity, sophisticated design, and a need for additional equipment; some even lack portability [16]. Among them, metal oxide semiconductor (MOS) gas sensors, working on the basis of changes in

* Corresponding author.
** Corresponding author. Division of Materials Science and Engineering, Hanyang University, Seoul, 04763, South Korea.
*** Corresponding author.
E-mail addresses: hyounwoo@hanyang.ac.kr (H.W. Kim), sangsub@inha.ac.kr (S.S. Kim), twk@hanyang.ac.kr (T.W. Kim).
[1] Equal contribution.

https://doi.org/10.1016/j.nanoen.2020.105369
Received 13 July 2020; Received in revised form 3 September 2020; Accepted 7 September 2020
Available online 17 September 2020
2211-2855/© 2020 Elsevier Ltd. All rights reserved.

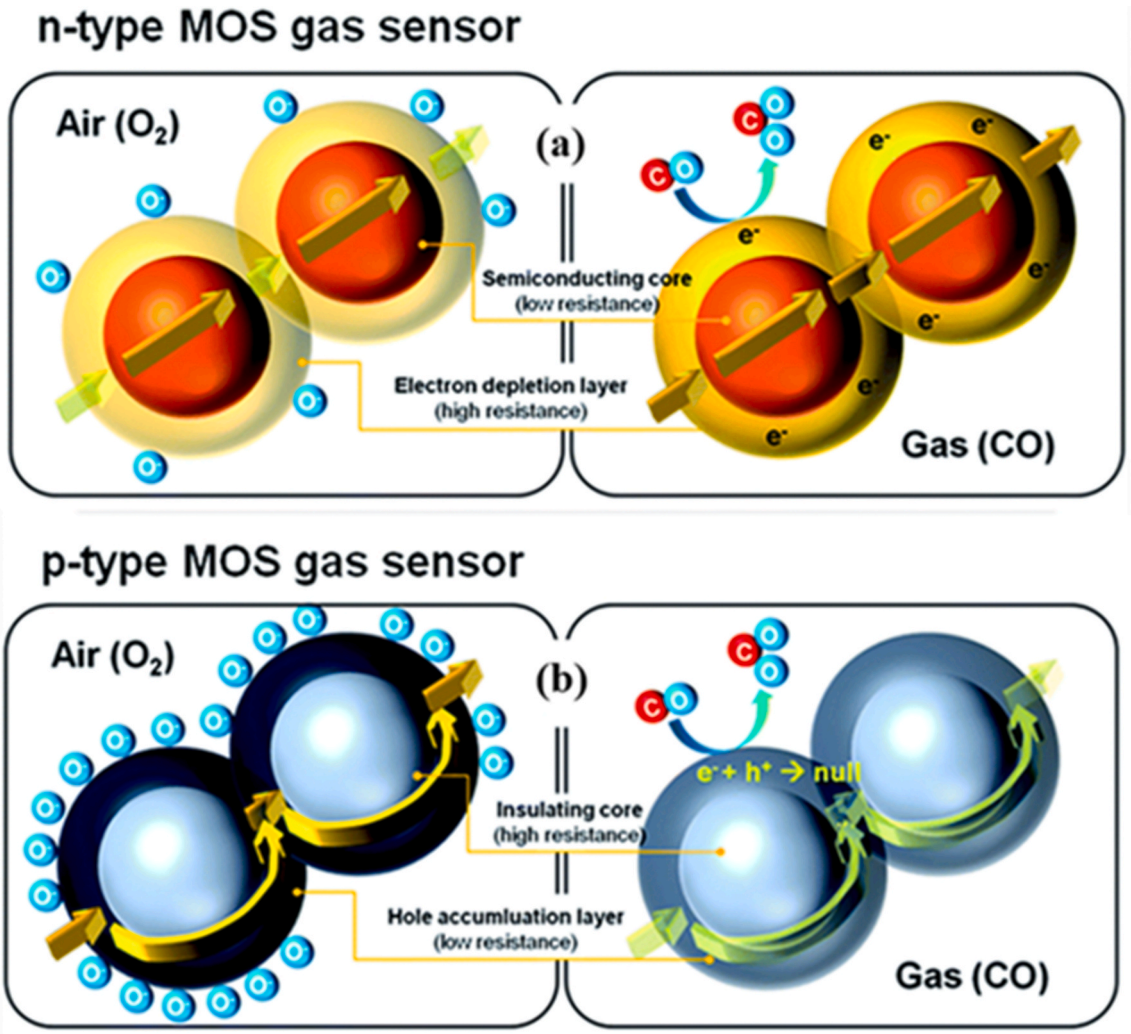

Fig. 1. Schematic illustration of the basic sensing principle for (a) n- and (b) p-type MOS gas sensors. Reprinted from Ref. [29] with permission from Elsevier (Copyright 2020).

resistance in the presence of a target gases, have attracted great attention and have become a hot research topic [17] because of their numerous and unique characteristics, such as high sensitivity, short response/recovery time, ease of fabrication, high stability, simple operation and low price [18,19].

The modulation of the electrical resistance or conductance in a target gas environment is known to be the basic gas sensing mechanism of a resistive-based sensor [20,21]. Initially in air, upon adsorption of oxygen molecules, an electron depletion layer (EDL) for n-type materials and a hole accumulation layer (HAL) for p-type materials will be formed on the sensor's surface. When an n-type MOS is exposed to an oxidizing gas, its resistance increases while for reducing gases the resistance decreases [22]. Fig. 1(a)-(b) schematically show the principle underlying the gas sensing mechanism of n- and p-type MOS-based resistive gas sensors [23].

The typical sensing mechanisms can be described by using the band bending theory. MOS materials are known to have many nanograins of different sizes and electrons are believed to flow in the grain boundaries. After oxygen gas molecules have been adsorbed on the sensor's surface, an electron will be extracted from the conduction band (CB), and an EDL will be formed in n-type MOS gas sensors [24]. This process results in energy-band bending as shown in Fig. 2(a). Due to presence of grains, Schottky barriers with a height of V_1 will be initially formed in air, as shown in Fig. 2(b) [25]. The reaction of oxygen ionic species with reacted gases can change the height of the Schottky barrier to (V_2) (Fig. 2(b)), which changes the conductivity, and thus the resistance, of the gas sensor [26–28].

Traditionally, chemiresistive-based sensors consist of three components: namely, the insulating substrate (typically alumina or silicon oxide), interdigitated electrodes, and a heater under the substrate to heat the sensor [31]. Generally, MOS-based gas sensors work at high temperatures (100–450 °C) [32]; however, this heating process results in some issues, such as degradation of the long-term stability due to the aggregation and coarsening of nanograins, an increase in fabrication cost due to the addition of the heater and high power consumption (100 mW up to 1 W) [33–36]. In this regard, power consumption is a challenging issue that limits the integration of MOS-based gas sensors into some important portable devices.

Due to the advances in smart phone technology, various sensors are now being integrated into cell phones for various applications, such as healthcare, public safety, and environmental and food monitoring [37]. The current chemiresistive sensors are not suitable for battery or portable operation due to the high temperatures needed for operation. Thus, the design of portable, low-cost and low power consuming or energy-saving gas sensors is essential for their use in wireless and portable devices [38,39]. Thus, many attempts, such as the uses of low-power light-emitting diodes (LEDs) [40], noble-metal functionalization [41] and hybrid materials [42], have been made to lower the energy consumption of gas sensors by decreasing the optimum sensing temperature. Moreover, two other promising techniques to reduce

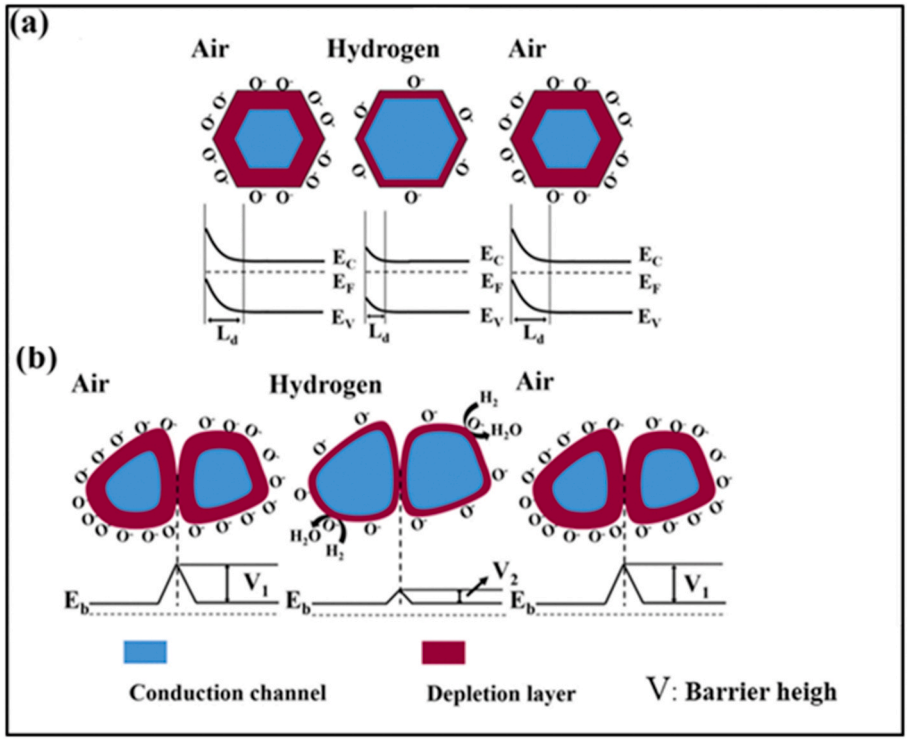

Fig. 2. (a) Schematic of the resistance change of an n-type MOS gas sensor during reducing gas (H_2) detection, (b) surface charge layer model, and (c) grain boundary barrier model. Reproduced from the Ref. [30] under the Creative Commons attribution 4.0 License (CC BY 4.0/). Copyright 2020, IOP Science.

power consumption significantly are operation of gas sensor in a self-heating mode [43] and integration of gas sensors into MEMS platforms [44].

In this review article, we have discussed the current advancements of energy-saving gas sensors based on chemiresistive principle (Fig. 3). This review article discusses several topics: self-heated gas sensors, low-power MEMS-based gas sensors, and gas sensors operating at room temperature with their applications including flexible/wearable gas sensors, and their associated gas sensing mechanisms. At the end, the review is concluded with brief summary and future perspectives on the possible opportunities for further developing energy-saving gas sensors.

2. Self-powered gas sensors

Piezoelectric nanogenerators (PENGs) and triboelectric nanogenerators (TENGs) enabling the monitoring of gases at RT in a self-powered way have been introduced by Zhong Lin Wang's group [45–47] In regard to PENG-based gas sensors, pure ZnO has been investigated, with the piezoelectric output being generated by ZnO acting as both a gas sensing signal and power supply [48,49]. Also, several metals, such as Cu [50], Pd [51], Au [52], and Pt [53], have been incorporated in order to enhance the catalytic reactions and, thus, the sensing performances. In addition, due to the many benefits, including increased modulation of the resistance, of ZnO-comprising heterostructures, including ZnO/SnO_2 [54], ZnO/NiO [55], and ZnO/In_2O_3 [56], they have been employed to enhance the sensing capabilities, providing excellent performances, owing to their stronger output signal [47]. TENGs can be used to monitor gases because the surface adsorbed species strongly affect the effectiveness of triboelectric charging [57]. The first TENG-based gas sensor was comprised of polymer films such as polyamide (PA) and polytetrafluoroethylene (PTFE) [57]. Subsequently, a variety of materials, such as ZnO [58], polyaniline (PANI) [59], and poly(3,4-ethylenedioxythiophene):poly(styrenesulfonate) (PEDOT:PSS) [60], has been adopted. Because we are dealing with chemiresistive-based gas sensors and the number of pages is limited, in this article, we will focus mainly on a special category of self-powered gas sensors, namely, self-heated gas sensors.

2.1. Self-heated gas sensors

As discussed, the energy consumption must be lowered if battery-operated gas-sensing devices are to be designed. In practice, for the gas sensors used in mobile or wireless network devices power consumption is in the range of several microwatts [27]. Typically, a conventional thick or thin film gas sensor equipped with a heater consumes about 1–5 W during its operation (Fig. 4(a)). On the other hand, MEMS-based gas sensors consume less than 30–50 mW to reach temperatures up to 500 °C. Also, for a self-heated gas sensor without an external heater, much less power is consumed [61]. The main factors underlying self-heating gas sensors are the application of an appropriate voltage, with Joule heating generating heat inside the sensor, thereby increasing its temperature. As shown schematically in Fig. 4(b), in this mode of operation, an external voltage is directly applied to the sensor electrodes. Nevertheless, for self-heated gas sensors, realization of high sensitivity at an appropriate bias voltage still remains a challenge [62].

The efficient self-heating (ESH) coefficient for a self-heated gas sensor can be expressed as

$$ESH = \Delta T / Q \quad (1)$$

where ΔT is the temperature increase due to the applied voltage, and Q is the electrical power dissipation. Typically, an ESH value greater than 1 (ESH > 1) is beneficial for self-heating, which means an increase of a few Kelvin/microwatt consumed. Conventional self-heating sensors ($\Delta T \sim 500$ °C and P ~ 10 mW) have ESH values of ~ 0.05 [63]. In general, MOS materials with nanowire (NW) morphology are preferred for self-heating studies [63]. As the NWs serve as pathways for electron transfer, the lengths of the NWs directly affect the heat generated inside the gas sensor, thereby allowing Joule heating to warm effectively the NWs and ensuring a higher response to the target gas. Furthermore, power is consumed at microwatt levels owing to the minimal thermal

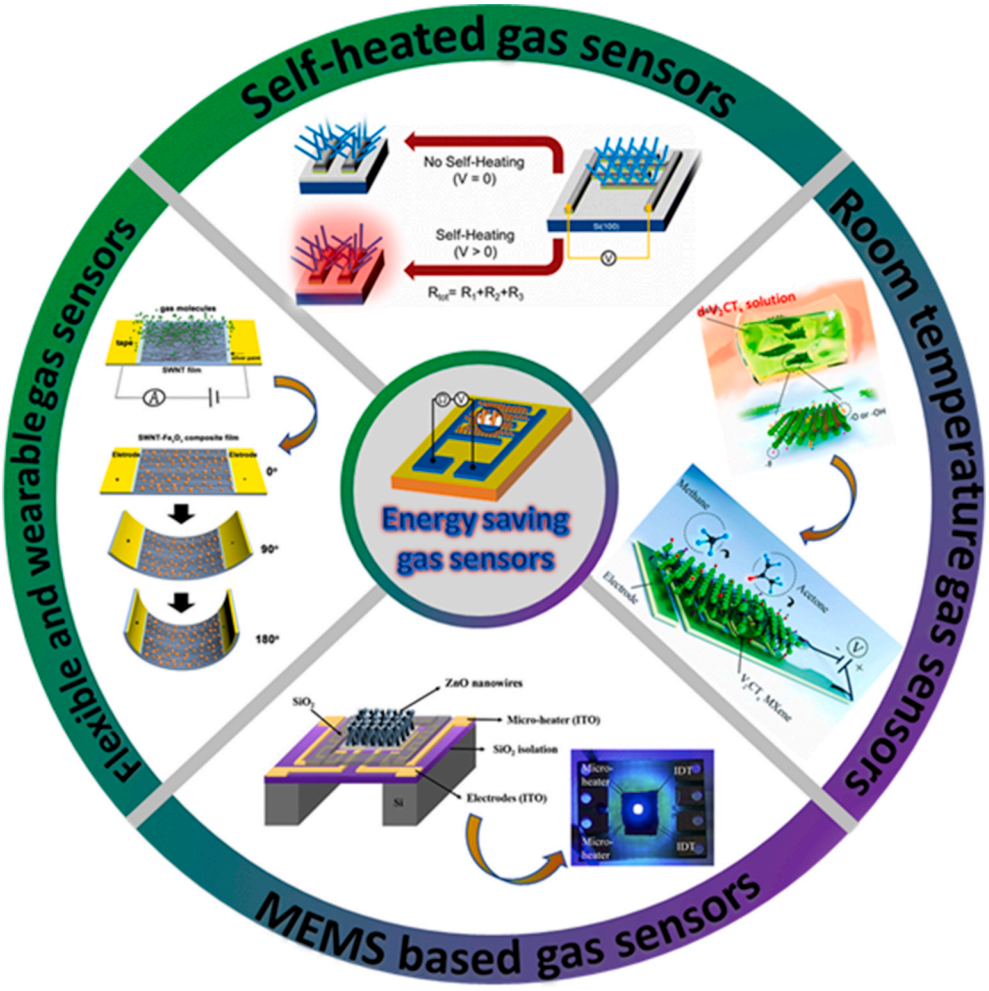

Fig. 3. An overview of the main techniques and applications of the energy-saving gas sensors discussed in this review paper.

capacitance of the NWs [32,65,66]. Moreover, the diameter of the NW is important because the temperature increase has an indirect relation with the radius of the NW; thinner NWs produce larger increases in the temperature [63].

In 2003 and 2006, Salehi et al. and Lee at al. introduced self-heated gas sensors based on SnO_2 and NiO thin films for the detection of CO and formaldehyde, respectively [64,65]. These systems showed lower power consumption as compared to conventional gas sensors. For further decreases in the energy consumption of the MOS gas sensors, NW morphologies are preferred due to the aforementioned advantages. The first NW-based self-heated sensor was introduced by Strelcov et al. [67], and so far, the self-heating properties of single NW [66,68–70], multiple NWs [67,68,71] and networked NWs [61,68] have been reported. As compared to the single-NW and the network-type NW sensors synthesized by using off-chip methods, on-chip NW sensors have many advantages [43,63,72,73]. Therefore, on-chip networked NW gas sensors are being developed for self-heating purposes; in this context, the on-chip methods are used to obtain power consumption at μW level [61, 67]. Hieu and co-workers reported the synthesis of on-chip grown networked SnO_2 NWs [74]. Prior to the on-chip growth, the electrode was designed using a photolithography method (Fig. 5(a)). After that, SnO_2 NWs having average diameters around 95 nm were grown using a well-known vapor-liquid-solid (VLS) method (Fig. 5(a)). The sensor showed a response of 2.1–2.5 ppm NO_2 gas with a power consumption of only 25 mW, along with good selectivity. The authors further addressed reducing the size of the electrodes with a gap width of 10 μm (Fig. 5(b)) and growing SnO_2 NWs on the electrode (Fig. 5(b-e)). The sensor exhibited an enhanced response ($R_g/R_a = 4.6$) towards NO_2 at 20 ppm. The sensing mechanism was explained based on modifications of the potential barriers at the SnO_2 NW-NW junctions and establishment of depletion layers at the SnO_2 NWs [75]. When the sensors were exposed to NO_2 gas, NO_2 molecules were adsorbed on the surface of the SnO_2 NW sensor, and electrons were extracted from the conduction band of SnO_2 NWs to form NO_2^- ionic species [76], which resulted in an increased number of depletion layers and potential barriers with increased heights.

The reduction of power consumption in the self-heated sensors depends on the sensing area of the electrode, and the design of head-to-head electrodes is an important aspect that is often neglected. Ngoc et al. introduced a self-heated NW gas sensor based on SnO_2 NWs grown using a chemical vapor deposition (CVD) technique, in which SnO_2 NW networks bridged the electrode gaps [63]. They investigated the effect of the electrode gap size on the sensing performance. For that purpose, the head-to-head electrodes gaps were maintained at 2, 5, 10 and 20 μm, which were labelled as G2, G5, G10 and G20, respectively. The mean diameter of the fabricated SnO_2 NWs was 80 nm. The electrode with a small gap was seen to yield a dense SnO_2 NW network (G2 with densest nanojunction) whereas the electrode with a large gap filled with a sparse network (G20) had the sparsest nanojunction. The sensor with a 20-μm electrode gap (G20) displayed a good response (3.75) toward C_2H_5OH (250 ppm) at a 10-mW power supplied. One of the merits in designing head-to-head electrodes is reduced power consumption because the self-heated sensor is dependent on the electrode area [74]. The nanojunctions between the SnO_2 NWs established the Schottky barriers, of

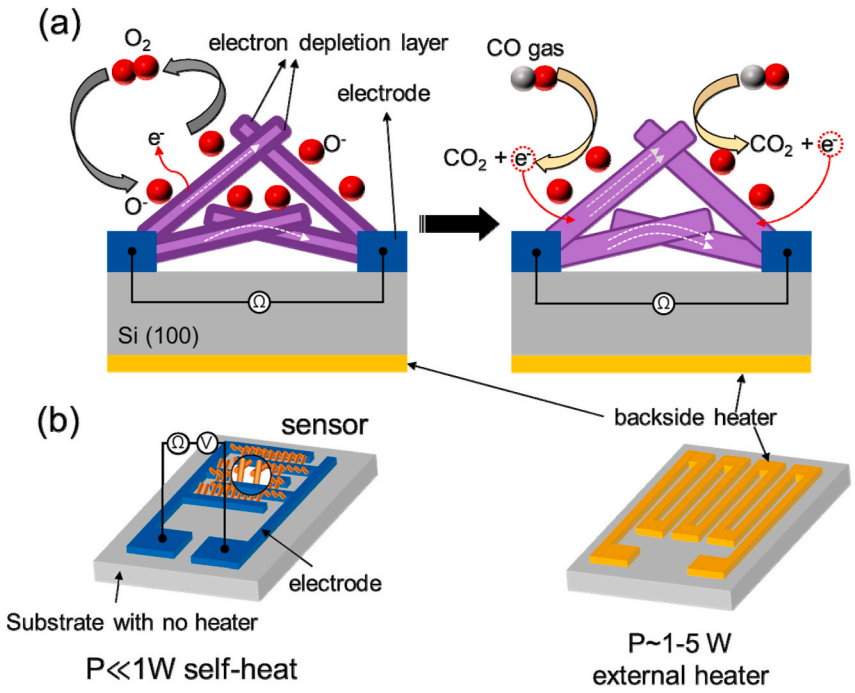

Fig. 4. Schematics of (a) a conventional MOS-based gas sensor and (b) a MOS-based gas sensor in the self-heating mode. Adapted from Ref. 62 with permission from Elsevier (Copyright 2020).

which increase the resistance at the nanojunction (R_j) as compared to the resistance at the NWs. Thus, one can conclude that for a self-heated NW sensor, warm-up at the junction in a nanoscale range is more important than network heating [67].

Noble metal decoration is a good strategy to enhance the gas sensing characteristics of MOS-based gas sensors, which is due to the sensitization effects of noble metals [77,78]. In this regards, the effect of self-heating and the density of the catalytic material were investigated in Ag-decorated SnO_2 NW networks by Ngoc et al. [33]. SnO_2 NWs were synthesized using a thermal evaporation method, and Ag nanoparticles (NPs) were sputter deposited on the surfaces of SnO_2 NWs for different durations of 10, 20, 40 and 80 s to control the density of Ag NPs; accordingly, the sensors were named ST10, ST20, ST40, and ST80, respectively. They used as H_2S gas sensor in the self-heating mode under different powers of 2–20 mW [33]. Among the four sensors, the ST80 sensor showed the highest response of 21.2 to 0.5 ppm to H_2S gas at a low heating power of 2 mW with an acceptable response/recovery time of 18/980 s. Ag NPs are known for their ability to selectively react with H_2S at low concentrations at temperatures below 200 °C [79]. However, when the power reached 20 mW, the authors reported serious thermal damage of the sensing material. When the sensor is exposed to H_2S gas, Ag_2O NPs react with H_2S gas molecules as follows:

$$Ag_2O + H_2S \rightarrow Ag_2S + H_2O \quad (2)$$

which is an exothermic chemical reaction that can occur at low temperatures. During the recovery period, the following reaction is expected:

$$2Ag_2S + 3O_2 \rightarrow 2Ag_2O + 2SO_2 \quad (3)$$

which is an endothermic chemical reaction occurring at high temperatures. Under low heating power, the reaction in Eq. (2) is dominant and converts Ag_2O into Ag_2S with a metallic nature, leading to a loss of the p-n junctions between Ag_2O and SnO_2 and decreased sensor resistance. Under high heating powers, the reaction in Eq. (3) increases, but never dominates the reaction in Eq. (2). Therefore, under lower heating powers, a higher gas response is observed. Also, with increasing Ag catalytic density, the response time decreases due to the high rate of the reaction between Ag_2O and H_2S while the recovery time increases because a longer time is required to change a large amount of Ag_2S back to Ag_2O [79–81].

In addition to Ag catalysts, Pt, Pd, and Au NPs have also been used in studies of self-heating gas sensors [82–87]. These noble metal NPs are generally functionalized on the surface of the gas sensor by using various approaches, such as UV-irradiation [88], γ-ray irradiation [89], and sputtering [90]. In a recent study of gas sensors operating in the self-heating mode, Kim et al. used UV-irradiation and sputtering techniques to deposit both Pd and Pt NPs on the on-chip grown ZnO NWs for a selective study of benzene and toluene gases [78]. Initially, the ZnO NWs were synthesized through a VLS method followed by ultraviolet (UV) irradiation technique to deposit Pd NPs while the Pt NPs were deposited by using a magnetron sputtering method, followed by an annealing treatment (Fig. 6 A). Morphologies of the synthesized Pd/ZnO NWs and Pt/ZnO NWs are shown in Fig. 6(B) and (C), respectively. For self-heating mode, both 5 nm-Pt-ZnO NWs and 5s-Pd-ZnO NWS sensors were studied with different applied voltages from 1 to 20 V. The Pt/Pd-ZnO NWs sensors showed high responses to toluene and benzene, respectively, among other reducing gases. The highest response of the 5 nm-Pt/ZnO NW sensor operating in the self-heating mode to 50-ppm toluene was 2.74 at RT under a 20-V applied voltage whereas the highest response obtained for the Pd/ZnO NW sensor under the same conditions towards benzene (50 ppm) was 2.20 (Fig. 6 D and E). Also, the power consumptions for the Pt- and Pd-ZnO NW gas sensors were found to be 208 and 139 μW at 5 V, respectively. The good selectivity toward benzene and toluene can be ascribed to the combination of catalytic effects of both Pt and Pd NPs, respectively. For benzene, the following reaction has been reported:

$$C_6H_6(g) \rightarrow C_6H_6(ads) \quad (4)$$

$$C_6H_6(ads) + 15O^- \rightarrow 6CO_2 + 3H_2O + 15e^- \quad (5)$$

and for toluene, the following reaction was reported:

$$C_7H_8(g) \rightarrow C_7H_8(ads) \quad (6)$$

$$C_7H_8(ads) + 18O^- \rightarrow 7CO_2 + 4H_2O + 18e^-. \quad (7)$$

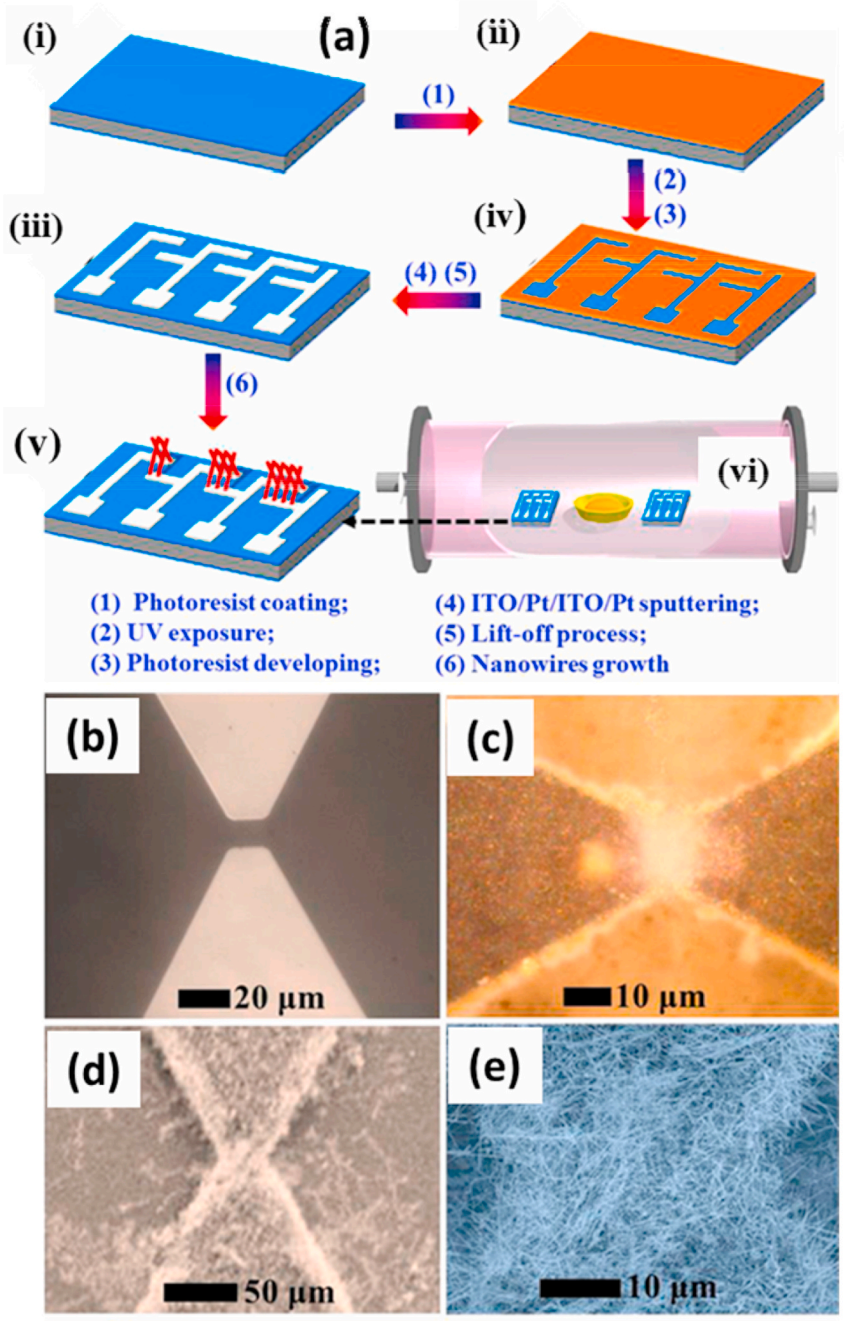

Fig. 5. (a) Schematic illustration of the fabrication of networked SnO_2 NWs. (b–e) FE-SEM images of networked SnO_2 NWs grown on the sensor substrate after reducing the electrode size. Reproduced from Ref. 74 with permission from the American Chemical Society (Copyright 2020).

Accordingly, the higher response of the Pt/ZnO NW sensor to toluene relative to the response of the Pd/ZnO NW sensor to benzene was related to the higher electron donating capacity of toluene. Schematic diagrams of the sensing mechanisms underlying pristine and Pt/Pd-ZnO NW sensors are provided in Fig. 6(F).

When a voltage is applied, heat is generated because the electrons lose kinetic energy when they collide with other electrons or other obstacles in their paths. The relation between Joule heating per volume (W/m^3) and the applied voltage can be expressed as follows [91]:

$$J=V^2/\rho L^2 , \quad (8)$$

where ρ is the resistivity of the sensing layer, and L is its length. The temperature increase due the self-heating effect was found to be 0, 1.6, 12.9, 25.8, and 80 °C, respectively, for applied voltages of 0, 1, 5, 10, and 20 V. Two possible locations of Joule heating were the ZnO grains and the networked ZnO-ZnO homojunctions [92].

Other than the single components, binary/ternary structures or heterostructures with different noble metal catalysts have been used for sensing studies due to the synergistic effect resulting from the combination of the MOS structure and a noble metal, which results in enhanced sensing reactions, surface activities and selectivities towards specific gases [93,94] Kim et al. reported Au-decorated SnO_2-ZnO core-shell NW-based sensors for the investigation of the CO gas-sensing properties under self-heating [83]. The SnO_2 NWs were synthesized vertically on chip by using the typical VLS method (Fig. 7a–b) [82]. Then, ultrafine Au NPs were deposited on the sensor's surface by using the γ-ray radiolysis technique (Fig. 7c). The ZnO shell thickness was varied from 10 to 80 nm by performing 50 to 500 cycles of atomic layer

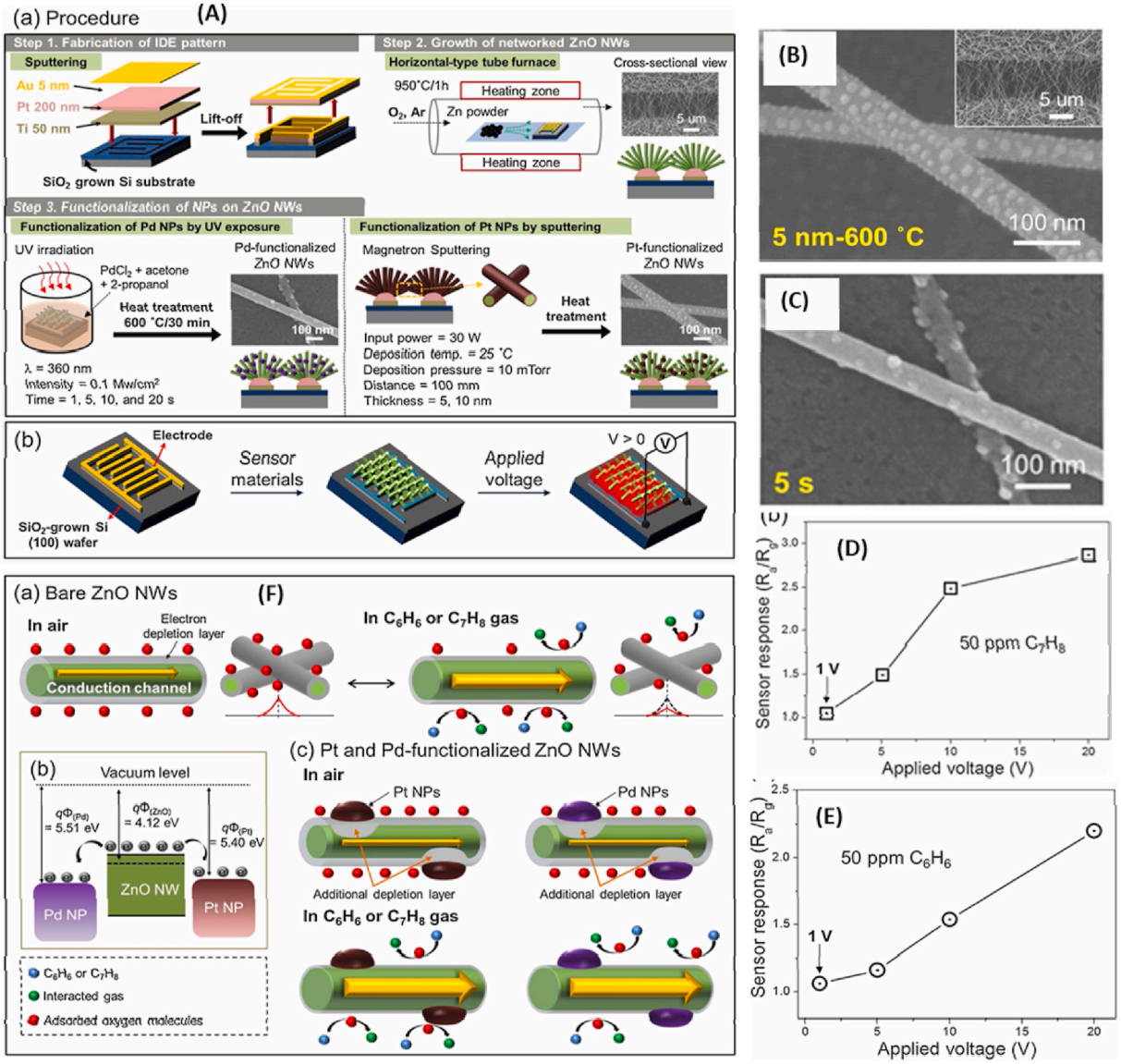

Fig. 6. (A) Scheme illustrating the procedures for the fabrication of the sensor chip (Step-1) followed by the on-chip growth of ZnO NWs (Step-II), and Pd and Pt functionalization on ZnO NWs (Step-III); (B, C) morphology of Pt and Pd-ZnO NWs; (D, E) response values obtained for Pt and Pd-ZnO NWs sensors with respect to applied voltages; (F) toluene gas-sensing mechanism of (a) pure ZnO NWs and (c) Pt/Pd-ZnO NWs. (b) Energy band diagram of Pt, Pd NPs and ZnO NWs. Reprinted from Ref. 82 with permission from Elsevier (Copyright 2020).

deposition (ALD). The relationship between the applied voltage (V > 1) and the increase in the temperature of the sensor due to the self-heating effect can be formulated as follows:

$$\Delta T = -1.3575 + 0.120V + 0.1645V^2 \text{ For } V > 1, \quad (9)$$

where ΔT is the increase in the temperature due to self-heating, and V is the applied voltage. Fig. 7(d) shows the variation in responses to CO (50 ppm) for different ZnO shell thicknesses under a 20-V applied voltage. With increasing ZnO shell thickness from 10 to 30–80 nm, the sensor showed increasing responses from 1.22 to 1.34 to 1.62, respectively.

The self-heating effects with different applied voltages from 0 to 20 V were checked, and the temperatures obtained 0–20 V were 23–103 °C (Fig. 7 (e)). The Joule heating process in the SnO_2-ZnO C-S NWs can contribute to three sources of resistances: (i) in the ZnO grains, (ii) in the grain ZnO boundaries, and (iii) through ZnO-ZnO homojunctions (Fig. 7 (f)). Accordingly, as the number of NW contacts in the sample increased with increasing thickest of the ZnO shell, the corresponding increase in the number of Joule heating sources led to a higher temperature and, thus, a higher gas response. Also, the good selectivity of the sensor to CO gas was related to a combination of the catalytic effect of Au, the special architecture of the sensor, and the sensing temperature (due to self-heating). However, the most important factor was the catalytic effect of Au to CO gas, where a low energy was required for oxidation of CO over Au NPs [82]. The lowest power for the sensor was found to be 0.81 nW at its corresponding voltage of 1 V whereas the highest power consumption of 8.3 μW was obtained at 20 V. The previous reports that we reviewed here are all showed energy consumption values from mW to μW. However, the obtained low power consumption in this study clearly indicates that Au/SnO_2-ZnO C-S NW sensors are very promising in the design of portable sensors with extremely low power consumption.

In addition to Au NPs, Pt and Pd NPs have been deposited on SnO_2-ZnO core-shell NWs to study their gas-sensing properties under self-heating conditions [85,86]. For example, Kim et al. reported SnO_2-ZnO C-S NWs (Fig. 8(a)-(c)) and studied the selective/sensitive detection of toluene gas without using external heating [84]. The SnO_2 NWs were synthesized by using a VLS method, whereas the ALD

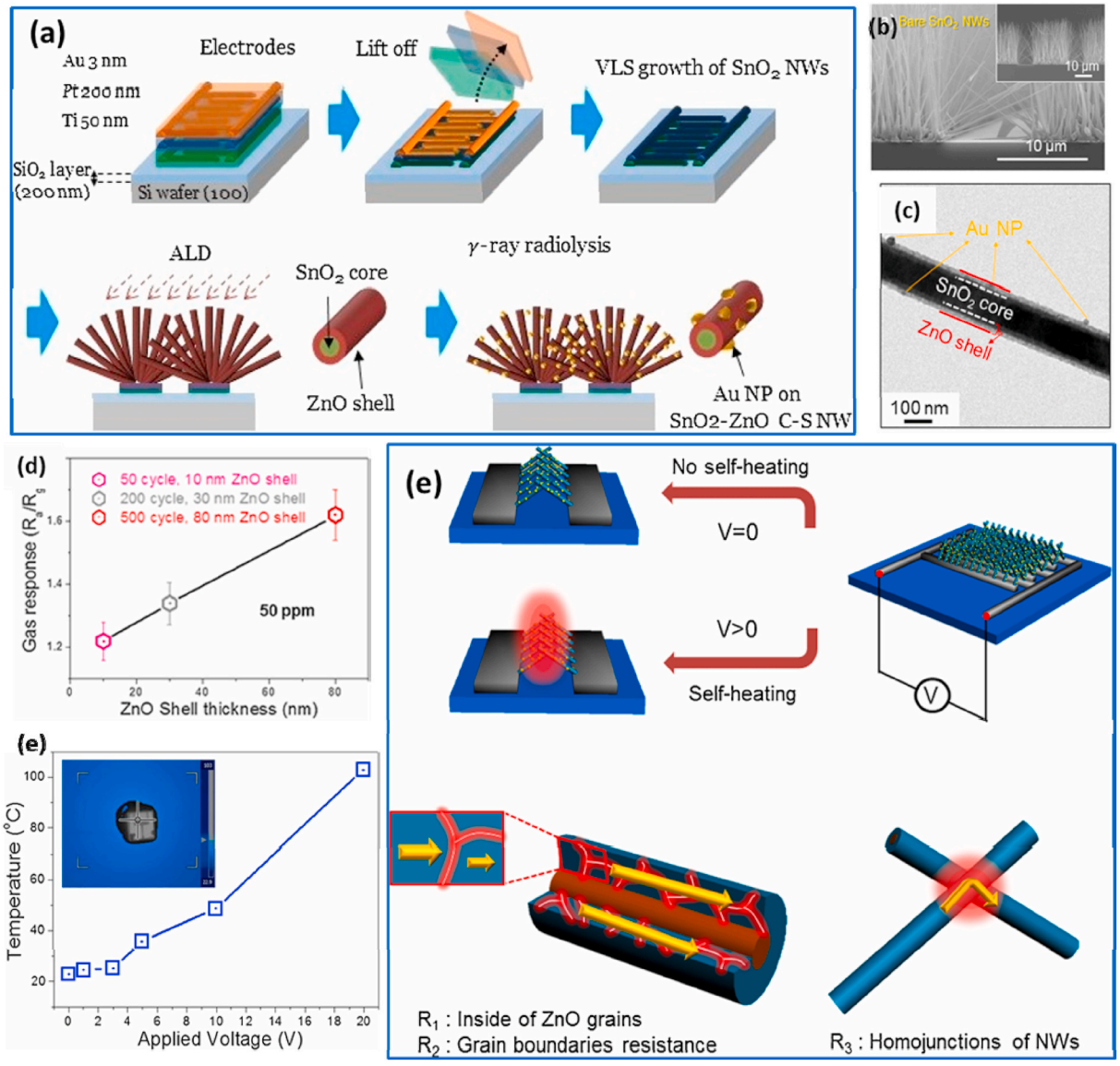

Fig. 7. (a) Schematic presentation of the synthesis procedures for Au-decorated SnO_2-ZnO core-shell NWs, (b–c) FE-SEM images of bare SnO_2 NWs and Au functionalized SnO_2-ZnO core-shell NWs, and (d) variation of Au/SnO_2-ZnO core-shell NW sensor's response with the thickness of the ZnO shell. (e) Temperature versus applied voltage and (f) schematic of the self-heating mechanism in SnO_2-ZnO C-S NWs and the corresponding process of resistance generation. Reprinted from Ref. 83 with permission from Elsevier (Copyright 2020).

technique was applied to coat a ZnO shell, followed by γ-ray radiolysis to deposit Pt NPs on the sensor surface. The thicknesses of the ZnO shells was set to 10, 30, and 85 nm for 50, 200 and 500 ALD cycles, respectively. Subsequently, the self-heating effect of Pt-decorated SnO_2-ZnO core-shell NW sensors having an 85-nm shell thickness was measured at different voltages from 0 to 20 V. Fig. 8(d) shows thermograph images obtained at 0, 1, 3, 5, 10 and 20 V. The 10-nm-thick shell shows a negligible self-heating effect whereas the 85-nm-thick ZnO shell sensor exhibits a quite good self-heating effect. The response of the Pt-decorated SnO_2-ZnO core-shell NW sensor with an 85-nm thickness to toluene was found to be 3.14. Moreover, the response of the sensor was explored at applied voltages from 1 to -20 V. The highest response of 3.14 was obtained at 20 V, and the lowest response of 1.00 was obtained at 1 V. The amount of power consumption of the as-prepared sensor was found to be 31 μW at 5 V, which provides promise for applications such as mobile and portable gas sensors. The mechanism of Joule heating can be explained based on mainly three possible sources (Fig. 8(e)). Firstly, the Joule heating occurs inside the ZnO grains as current flows through them. Secondly, the Joule heating occurs in the ZnO grain boundaries. Thirdly, due to the entangled NW structure of the NWs, it occurs in the ZnO-ZnO homojunctions as electrical currents flow through those homojunctions [82]. The sensing mechanism in Fig. 8(e) shows the formation of heterojunctions between ZnO/Pt and ZnO/SnO_2, which greatly affect the sensing response.

To further continue their self-heating study, Kim et al. reported on-chip grown SnO_2 NWs Si/SiO_2 substrate by using a VLS technique for ultra-low power consumption sensors in the nW range when operating in the self-heating mode [85]. The ZnO shell, which had an 80-nm thickness, coated on SnO_2 NWs by using the ALD method, after which the Pd NPs were coated on the SnO_2-ZnO core-shell NWs by using γ-rays radiolysis. The heat produced because of Joule heating is known to be directly proportional to the voltage and indirectly to the resistance according to following formula:

$$Q \propto V^2/R \tag{10}$$

Thus, Joule heating can be increased by increasing the applied voltage. The responses of a Pd-SnO_2-ZnO core-shell NW sensor toward

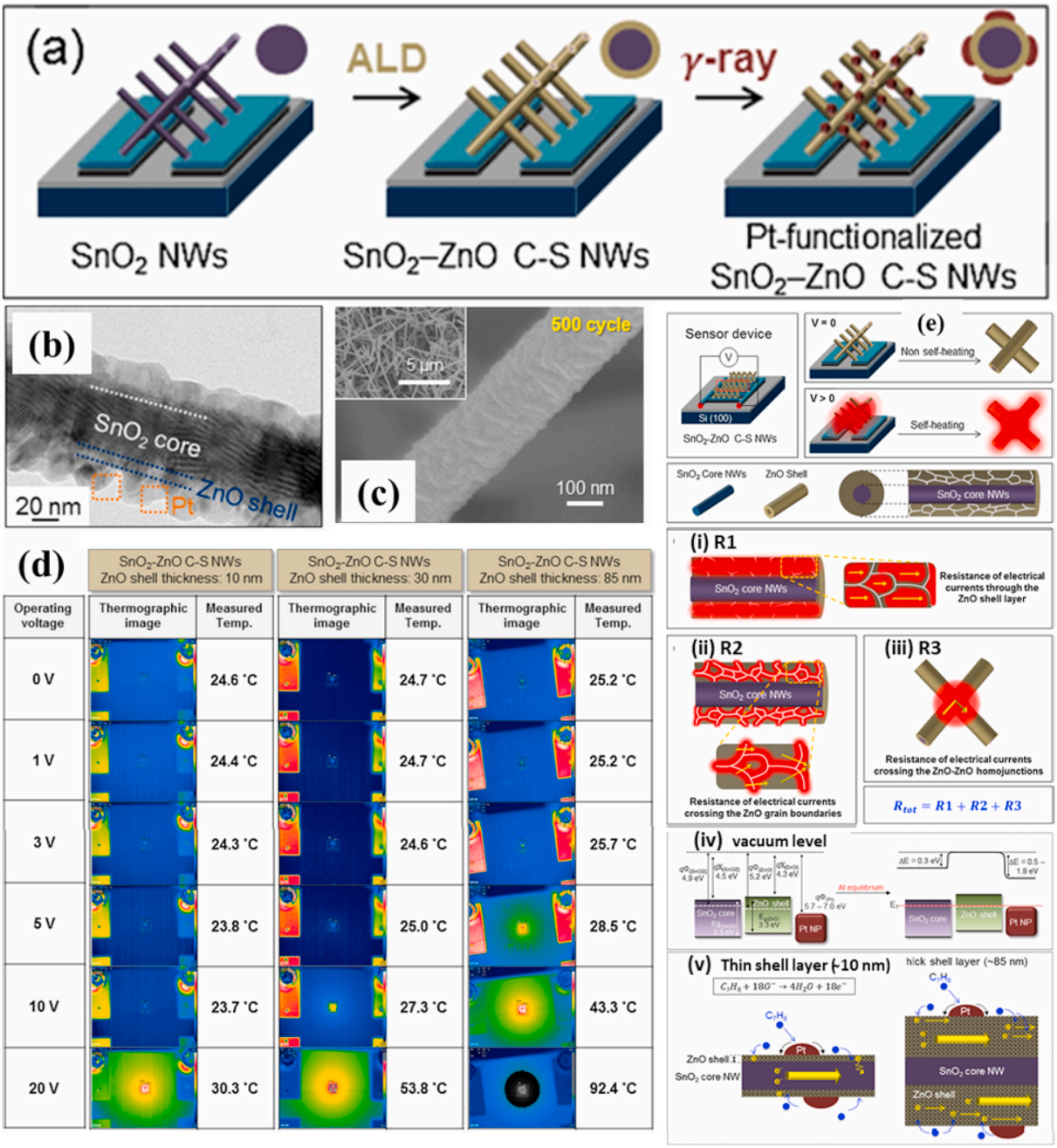

Fig. 8. (a) Synthesis procedure for realizing Pt-SnO_2-ZnO C-S NWs, (b, c) corresponding FE-SEM images, (d) thermographic images of Pt-SnO_2-ZnO C-S NW sensors for different shell thicknesses (10–85 nm) with varying operating voltage (0–20 V), and (e) self-heating and sensing mechanisms. Reproduced from Refs. [84] with permission from Elsevier (Copyright 2020).

benzene at different concentrations were measured under different applied voltages from 1 to 20 V. With increasing concentration and applied voltages, the response also increased, and the highest response of 2.62 was obtained for 50-ppm benzene at 20 V. The high selectivity of the Pd-SnO_2-ZnO core-shell NW sensor toward benzene can be attributed to the interaction between the π electrons of benzene and the d-band electrons of Pd NPs [76]. A response of 43.13 was obtained for 50-ppm benzene at a temperature of 200 °C. The response of the sensor was mainly attributed to the ZnO shell because the heterojunction barrier hinders the electron flow from SnO_2 to ZnO. Therefore, the majority of electrons flow through the ZnO shells. The Joule heating in SnO_2-ZnO C-S NWs typically occurs in different ways viz. inside the ZnO grains and grain boundaries as well as the ZnO-ZnO homojunctions. The highest value of power consumptions of 22.6 μW was obtained at 20 V whereas the lowest value of 0.99 nW was obtained at 1 V.

So far, only n-type MOS materials were discussed for sensing studies. This is due to the fact that in general, p-type MOS-based gas sensors show lower responses relative to those of their n-type counterparts [95]. However, a few studies of p-type gas sensors operating in the self-heating mode have been published. Among many p-type MOS materials, CuO has been investigated for H_2S sensing due to its being highly sensitive to H_2S [96,97]. Kim et al. prepared pristine (Fig. 9(a)) and Pd-functionalized CuO NWs (Fig. 9(b)) for H_2S gas sensing in self-heating mode (1–5 V) as shown in in Fig. 8(c) [86]. The Pd functionalization on the CuO NWs (Pd/CuO NWs) was carried out using ultraviolet irradiation (Fig. 9(d)). The Pd-functionalized CuO NW sensor was seen to exhibit its best response of 1.894–100 ppm H_2S gas at 5 V which was higher than that of pristine sensor (Fig. 9(e)). The high

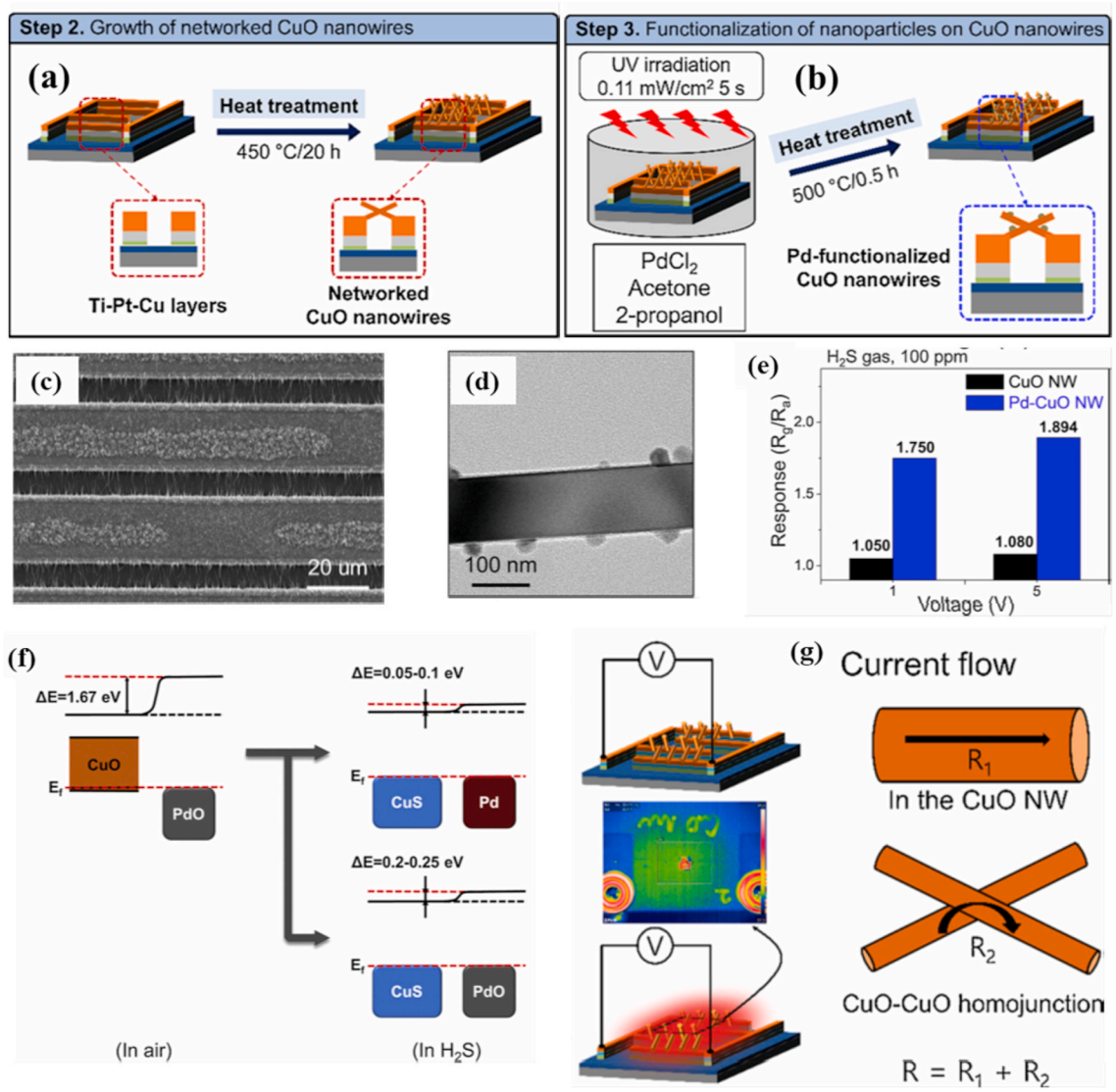

Fig. 9. (a) Schematic for the preparation of Pd-decorated CuO NWs. TEM micrographs of the as-synthesized (c) CuO NWs and (d) Pd/CuO NWs. (c) Heat generated under the self-heating condition and the corresponding thermographic image of the CuO NW sensor at 5 V. (d) Self-heating mechanism of the CuO NW sensor showing the self-heating effects in CuO NWs and CuO-CuO junctions. Reproduced from Ref. [86] with permission from Elsevier (Copyright 2020).

sensitivity of the current sensor was ascribed to the transformation of CuO to CuS with metallic conductivity during exposure to H_2S (Fig. 9 (f)). The change in conductivity from CuO (E_g =1.2 eV) to CuS and the catalytic effect of Pd NPs resulted in a high response to H_2S gas, in accordance with literature [97]. The self-heating effects were attributed to two phenomena (Fig. 9(g)), (i) the passing of electrons through the CuO NWs and (ii) the CuO-CuO homojunctions network, in which the homojunctions were in direct contact with one another. Thus, the Joule heating was generated in the CuO-CuO homojunctions network [83,98], leading to temperature increase inside of the sensor and appearance of a sensing signal.

In an another experiment, a p-type MOS material was synthesized by oxidizing metal NPs such as Pt NPs. Prajapati et al. reported on the use gas sensors with a single NW of PtO_x and a NW array of PtO_x/Pt for H_2 sensing at RT under a self-heating condition [99]. The diameter of the Pt NW arrays was varied from 10 to 80 nm. For the formation of a single PtO_x NW, a 60-nm Pt NW was oxidized in an oxygen ambient under a constant voltage. Upon exposure to hydrogen gas, the single NW PtO_x sensor showed an excellent response ($\Delta R/R_a \times 100$) of about 818% to H_2 (1000 ppm) at RT under an ultra-low 0.25-V applied voltage. However, the NW array of PtO_x/Pt showed a higher response (~936%) with a quicker response/recovery time of ~25 s/~108 s under the same conditions. The higher sensitivity and the faster response of the oxidized NW array were related to the increased sensing area and the different oxidation lengths. The oxidation (PtO_x) length of the PtO_x/Pt NW array was 50 nm to ~100 nm, which facilitated a reduction in the response time with the electrode having a nanoscale gap while the higher oxidation lengths (500 nm–1 μm) offered higher surface areas for gas sensing.

Other than NWs, two dimensional (2D) nanosheets (NSs), especially 2D layered transition metal dichalcogenides (TMDs) have been also used for self-heating studies due to their several unique properties [100,101]. In this context, Kim et al. prepared Au NP decorated WS_2 NSs (Fig. 10 (a)-(b)) for CO sensing in the self-heating mode [87]. Microscopically analyses which are shown in Fig. 10(c-e), demonstrate the formation of desired morphology. The actual sensor temperatures were obtained using an IR imaging camera (Fig. 10(f)), and the sensor showed its highest response to CO gas at only 2 V (Fig. 10(g)) with a power consumption of only 28.6 μW. The very low power consumption was related to the intrinsic resistivity of WS_2 NSs, which facilitated heat generation within the WS_2 NSs. In addition, many WS_2-WS_2 homojunctions acted as power sources of Joule heating upon application of a voltage. The good

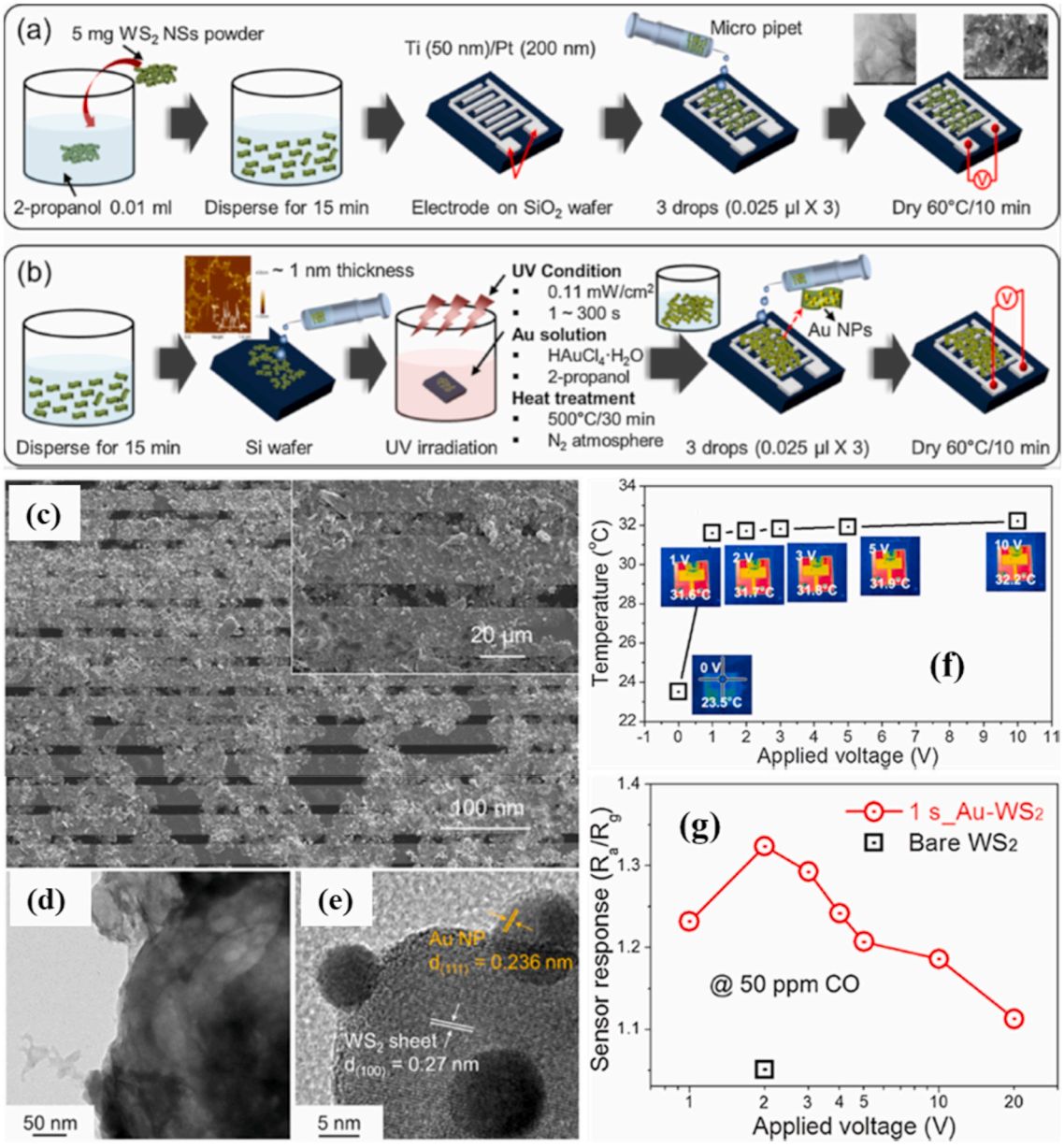

Fig. 10. (a, b) Schematic presentation of the synthesis procedures for pristine and Au-decorated WS_2 NSs, (c) FE-SEM micrographs of pure WS_2 NSs on the sensor substrate, (d) TEM micrograph of pure WS_2 NSs, (e) high-resolution TEM image of Au-decorated WS_2 NSs, (f) variation of the temperature (irradiated for 15 s) with respect to the applied voltage, and (g) response to 50-ppm CO versus applied voltages (irradiated for 1 s). Reproduced from Ref. 87 with permission from Elsevier (Copyright 2020).

response was related to the catalytic role of Au towards CO gas at low temperatures.

Also, MOS materials with nanorod morphology have been used for self-heating studies. For example, Seo et al. and Choo et al. designed self-heated gas sensors with high-sensitivity to H_2 [102,103]. A cost-effective, self-heating (2–8 V), ZnO-based H_2 gas sensor was made from ZnO nanorods grown using a hydrothermal process on the surface of indium tin oxide (ITO) [103]. Joule heating was mostly generated inside the ITO whereas ZnO acted as a resistor to modulate the electrical resistance of the sensor. At 4 V, evidence of Joule heating in the sensor was obvious, and with further increases in the operating voltage, higher temperatures were obtained for the sensor. At a maximum 8 V, the working temperature was 75 °C, and the highest gas response to H_2 was the result. However, no selectivity study was performed.

The above section can be summarized as follows: the reasons for operating the gas sensors in the self-heating mode are to overcome the issue of integrating a heater element and to lower the power consumption. Mostly MOS materials with NWs morphology, including single NW, multiple NWs and networked NWs, have been used for self-heated gas sensors. However, the design of the individual NW sensors involves complicated process steps and laboratory fabrication methods with low yield, which are hardly transferable for large-scale production [68]. Also, core-shell NWs are very promising for use in the self-heating mode due to maximization of the interfaces between the core and the shell. Sensing materials decorated with noble metals can operate with low power consumptions due to their high sensitivity resulting from the presence of the noble metals. Table 1 shows the properties and the power consumptions of some self-heated gas sensors reported in the literature.

Table 1
Summary of different self-heating gas sensors showing their sensing properties and power consumptions.

Sensing materials	Target gas and conc. (ppm)	Power consumption	Applied voltage (V)	Sensitivity (S) [R_a/R_g or R_g/R_a *[$(R_a-R_g/R_a) \times 100$]	Ref.
Ag decorated SnO_2 NWs	H_2S (0.5)	2 mW	–	21.2	[33]
SnO_2 NW networks	NO_2 (1)	1 μW	–	3.2	[38]
SnO_2 NW	NO_2 (10)	10 μW	–	1.3	[38]
Pt-coated $W_{18}O_{49}$ nanowire networks	H_2 (50)	30–60 mW	6	~1.1	[61]
SnO_2 NWs	C_2H_5OH (100)	10 mW	–	3.75	[63]
SnO_2 thin films	CO (1000)	0.1 W	10 (ac)	1.01	[64]
SnO_2 individual nanowires (r < 45 nm)	NO_2 (0.5)	27 μW	–	1.01	[66]
SnO_2 individual NW	NO_2 (40 ppm)	35 μW	25 V	21.3	[67]
SnO_2 multiple NW	NO_2 (40)	90 μW	40 V	–	[67]
SnO_2 networked NW	NO_2 (40)	56 μW	40 V	–	[67]
Pd-SWCNTs	CH_4 (6)	few μW	–	1.02	[68]
networked SnO_2 NWs	NO_2 (2.5)	25 mW	1	25.6	[74]
Pt-coated SnO_2–ZnO core–shell NFs	C_7H_8 (50)	31 _W	3	1.41	[84]
Pd functionalized SnO_2-ZnO core-shell NWs	C_6H_6 (50)	22.6 μW	20	1.62	[85]
Pd functionalized CuO NWs	H_2S (100)	-	5	1.894	[86]
Au-decorated WS_2 nanosheets	CO (50)	28.6 μW	40	1.48	[87]
Pd functionalized carbon NWs	H_2 (1000)	30 μW	–	1.2	[102]
WO_3 nanocolumnar thin films	NO_2 (1)	21.6 μW	5	~130	[104]
Ti NPs decorated MWCNTs	O_2	10–100 μW	0.5	1.1 (10 mTorr)	[105]
Pd functionalized Si NWs	$H_{2\ (10,000)}$	Few μW	1.7	1.65*	[106]
Pd functionalized carbon NWs	H_2 (1000)	30 μW	–	1.2	[107]
Suspended SWCNTs	NO_2 (1)	2.9 μW	5	1.8	[108]

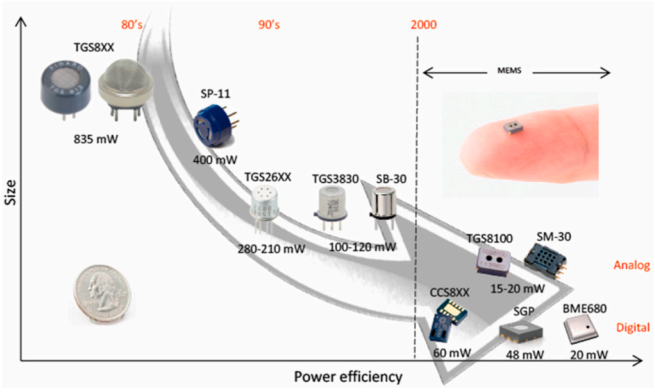

Fig. 11. Recent progress on the miniaturization of sensors with respect to their power efficiency. Reproduced from Ref. 112 (MDPI) under the license of creative commons attribute (https://creativecommons.org/licenses/by/4.0/).

3. Low-power MEMS-based gas sensors

During the fabrication of sensing devices, MOS sensors are connected to a heater, which is necessary to activate the sensing reaction between the target gas and the sensing material. Therefore, many MOS-based commercial gas sensors use heater resistors to warm the sensing surface to the desired temperature [109]. However, the power consumption of such gas sens0rs is high [110], which limits their application to smartphones and portable electronic devices. Therefore, a micro heater with low power consumption can play a vital role in overcoming the above issue [111]. The recent advances in different fabrication technologies have lead to the downsizing of sensing chips and heater resistors, resulting in tiny, reduced-power gas sensors (Fig. 11). Especially, the micro-electromechanical system (MEMS) has enabled very compact, low power consuming (a few tens of mW), MOS gas sensors to be fabricated [112].

Gas sensors based on MOS materials can be integrated into MEMS platforms to achieve miniaturized and portable sensing devices with very low power consumptions. MEMSs are electro-mechanical systems with a 3D geometry. They are constructed on silicon-wafer platforms by using microelectronic fabrication of a photolithography method and post-process techniques. These processes allow designers to accumulate different sensor arrays on a single sensor platform that can be utilized for mass-production at a low cost [113]. Nanoscale MOS materials integrated with MEMS technology are widely employed in gas sensing applications due to the drastically reduced size, low cost and significantly lower power consumption of such devices [114–116]. In comparison with traditional MOS-based gas sensors (Fig. 12(a)), MEMS-based gas sensors that use MOS materials typically consist of three basic components: (i) a micro-heater, (ii) a sensing material in the form of a thin film (receptor layer), and (iii) interdigited electrodes (Fig. 12(b)). The micro-heater embedded in the substrate layer (suspension), a dielectric layer or an insulation layer, a passivation layer, and a microheater element, as shown in Fig. 12(c-e), are components of a conventional MOS gas sensor [117,118]. Different materials, such as platinum (Pt), nichrome (Ni) and tungsten (W), can be used for the fabrication of the heater part [119–121]. Five categories of microheater geometries are typically used: rectangular, square, circular, irregular shapes (like honeycombs, drive wheels or others), and 3D structures. The most widely reported structure is the meander shape with either a square or a rectangular pattern [122]. Microheaters can be categorized into different configurations, such as a closed membrane, a suspended membrane or a bridge (Fig. 12(c)–(e)). In all of them, the substrate just below the sensing region is etched away. Among them, the suspended membrane substrate (Fig. 12(d)) is the most popular because of its much reduced power consumption [123]. The suspended membrane may either be released from the front side (Fig. 12(f)) or the back side (Fig. 12 (g)). The main aim in making bridge/diaphragm architecture is to reduce the heat loss through air, which has a low thermal conductivity: 0.026 WK^{-1} m^{-1} at 20 °C, by using thermal isolation, thereby inducing low power consumption. The back-side etching of a substrate is good due its simplicity compared to front side etching because the front side etching for creating the cavity needs extra protection of the structure layer or the sacrificial layer.

MOS-based MEMS gas sensors were first realized in the early 1990s and were derived from the so-called micro-hotplate devices [124]. Many reports on MOS-based MEMS gas sensors have been published [111, 125–127]. For example, Hsueh et al. fabricated a transparent MEMS-type gas sensor (Fig. 13) based on ZnO NWs (length: 2.5 μm, diameter: ~75 nm) synthesized using a hydrothermal method as the sensing material, ITO as a transparent electrode, and a micro heater [127]. The highest power consumption at an applied voltage of 6.73 V was only 124 mW whereas the maximum power consumption obtained at an applied voltage of 11.55 V was 386 mW. The temperature obtained

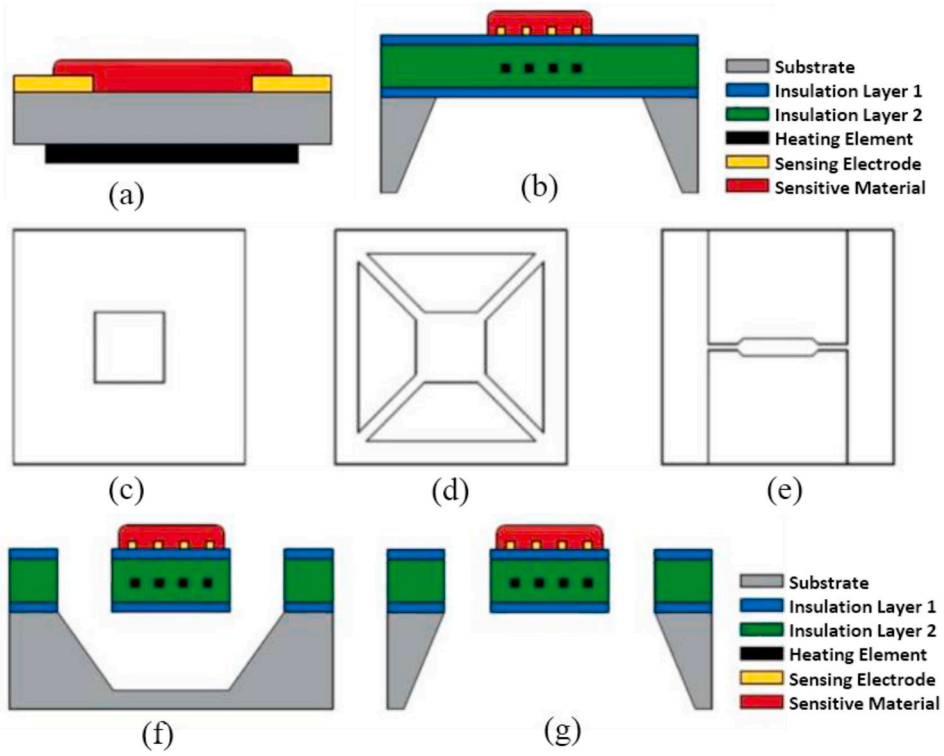

Fig. 12. (a) Schematic diagrams of all the components of a conventional MOS gas sensor, (b) a MEMS-based MOS gas sensor. Schematic diagrams of different configurations of a MEMS based MOS gas sensor, (c) closed, (d) suspended, and (e) bridge membrane (e), and schematic diagrams of suspended microheater with (f) front side, and (g) back side etching. Reproduced from Ref. 118 with permission from MDPI (Copyright 2020).

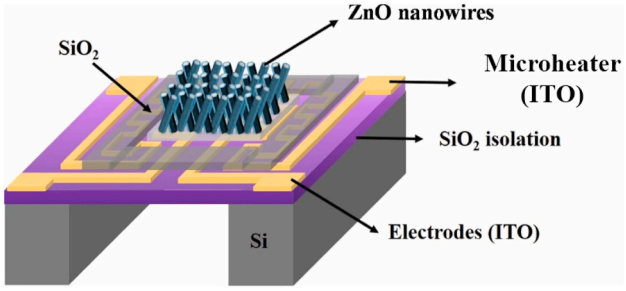

Fig. 13. Schematic illustration of a ZnO NW-based MEMS sensing device. Reproduced from Ref. 127 with permission from Elsevier (Copyright 2020).

at 6.73 V was 150 °C, and that obtained at 11.55 V was 350 °C. The sensing results showed that the response to NO gas was higher than the responses to other gases due to the fact that the bond energy of NO (N–O = 200 kJ/mol) is lower than those of other gases. Also, a blue-light-emitting diode (LED) was integrated into the MEMS sensor, and its lighting effects on the gas-sensing characteristics at RT were investigated. When the LED was switched on, the sensor current increased while it decreased when the LED was switched off, which was related to the presence of defects in the ZnO NWs. A large number of electrons were generated by LED-emitted light, and the presence of defects and photo-generated electrons led to an enhanced response to NO gas.

MOS composites have also been used in MEMS configurations to enhance the sensitivity of MEMS-based gas sensors. Behera et al. synthesized p-n ZnO-CuO nanoflake heterojunction nanostructures based on a MEMS platform (Fig. 14 (a) and (b)) [128]. The simulated temperature distribution profile of the microheater indicated that the heat was uniform throughout the substrate and confined within the sensor platform (Fig. 14(c)). At an increased sensing temperature of 259 °C, the sensor consumed only 100 mW of power. At 300 °C, the sensor exhibited a high sensing response [$(\Delta R/R_a) \times 100$] of ~275% to 50 ppm of acetone. The enhanced gas-sensing performance was attributed to the charge carrier modulation at the surfaces of ZnO and CuO, the barrier height modulation at the ZnO-CuO interface, the presence of defects in the interfaces between ZnO and CuO, the catalytic effects of CuO, and the higher dipole moment of acetone relative to those of other gases.

MOS-decorated gas sensors also have been used in MEMS configurations. For instance, Yuan et al. reported a MEMS-based acetone sensor made from CeO_2 nanodots decorated on WO_3 NWs, prepared through a hydrothermal and subsequent thermal decomposition [129]. The sensor exhibited a response (R_a/R_g) of 1.30–500 ppb acetone with good stability, which indicates that this sensor can be used to diagnose diabetes via breath analyses. The sensing mechanism was related to the high surface area of the gas sensor, the fast carrier transport of the WO_3 NWs, the formation of WO_3-CeO_2 heterojunctions, and the existence of large numbers of oxygen vacancies in CeO_2.

In summary, even though gas sensors based on MEMS technology can operate with reduced power consumption, the slurry-based drop coating of sensing materials on the small sensing areas of MEMS micro hot plates is an extremely difficult task. Furthermore, fabrication of MEMS-based sensing devices on a large-scale has difficulties such as low yield and large sample-to-sample deviation, which ultimately limit their practical use. One good strategy to deal with this is to deposit the sensing material by using advanced physical techniques such as sputtering, which is a simple technique, to integrate the sensing materials on micro-hot-plate platform [130].

4. Low or room-temperature operated MOS gas sensors

So far we reviewed the MOS-based gas sensors in self-heating mode without external heater. Mostly, various MOS materials with NW morphology have been reported for operation in self-heating mode. However, a very few reports on other kinds of morphologies based on

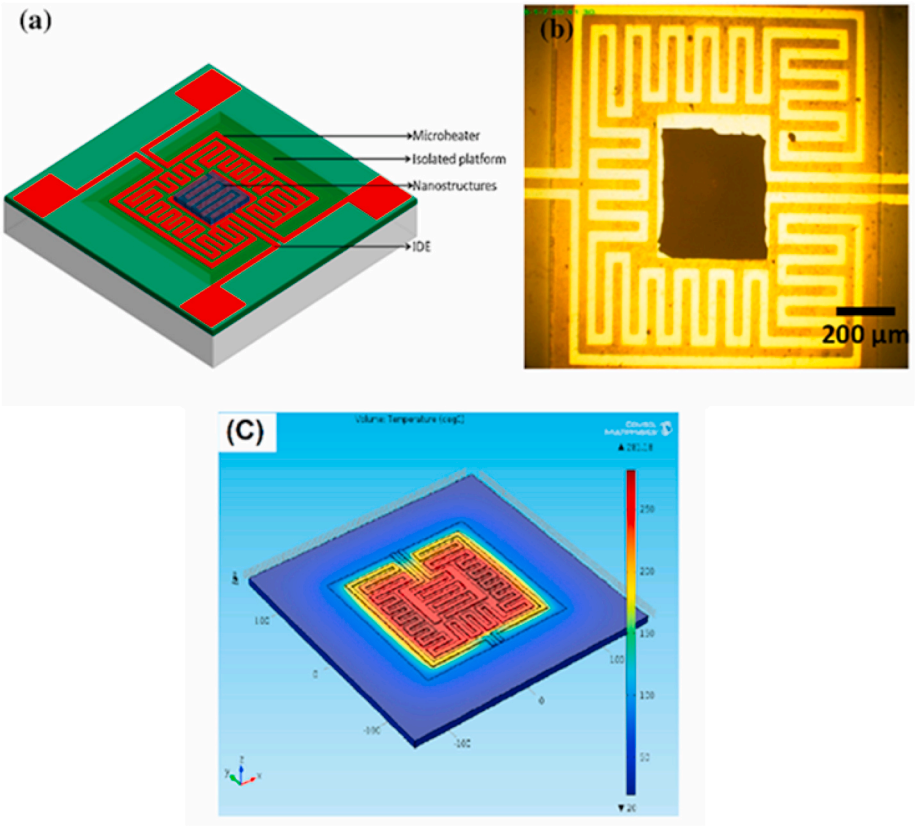

Fig. 14. (a) Schematic and (b) photographic image of a MEMS-based gas sensor. (c) temperature distribution of the microheater. Reproduced from Ref. 128 with permission from Elsevier (Copyright 2020).

self-heating method for gas sensing application have been also published [87,102,104].

Conventional MOS-based gas sensors usually operate at high temperatures ranging from 100 to 450 °C in order to achieve enhanced sensing performance because of their larger band gap [77,131], which leads to serious problems such as high-power consumption and increase of overall price of the gas sensor due to need for the heater. Thus, RT operation of gas sensors is highly desirable to minimize the risk of gas explosion, reduction of energy consumption, increases sensor life and possibility of integration into smart phone devices [132,133]. Recently, many strategies have been carried out to enhance the sensing properties at MOS gas sensors RT such as morphology engineering of pristine MOSs [134–136], noble metal NPs-decorated MOSs [137,138], doped MOSs [139,140], construction of heterojunction structures [141,142], hybrid composites with conducting polymers [143], carbon materials [144–146] and 2D materials such transition metal chalcogenides, metal carbides [147,148]. Also UV-irradiation is a good technique to reduce the sensing temperature [149,150]. In following section we discuss about low temperature or RT gas sensors based on MOS materials.

4.1. Pristine MOS gas sensors

It is known that morphology greatly affects the gas sensing properties, and therefore various morphologies have been used for sensing studies [151]. For example, Wang et al. prepared WO_3 hierarchical hollow spheres by a facile hydrothermal method and explored its NO_2 sensing properties at RT [152]. The sensor exhibited a high response (R_g/R_a) of 15.1 to 300 ppb NO_2 gas with excellent selectivity and moderate response/recovery times (670 s/2940 s) and good repeatability. The high NO_2 sensing performance of the sensor was related to the large surface area, presence of high oxygen vacancies and electronic interactions which occurred between NO_2 gases with the oxygen ions on the surface of the sensor and electronic interactions occur between target gases with the oxygen ions of the sensor [153–155].

In addition to n-type MOSs, p-type MOSs has also been studied for RT gas sensing. For instance, Li et al. reported a highly sensitive and selective H_2S gas sensor using porous CuO nanosheets, synthesized using a hydrothermal method [135]. The sensor exhibited a response of 1.25 towards 10 ppb H_2S with response/recovery time of 234 s and 76 s and excellent selectivity to H_2S. According to the literature p-type CuO is the dominant material for H_2S sensing [156]. The sensing mechanism was mainly related to the transformation of semiconducting CuO to metallic CuS. In fact, H_2S molecules can react with CuO to form CuS, based on the following reaction [156].

$$H_2S\ (g) + CuO\ (g) \rightarrow CuS\ (s) + H_2O\ (g) \quad (11)$$

The transformation to CuS was confirmed by using XPS analysis, where after exposure to H_2S gas a new peak related to the Cu $2p_{3/2}$ state at 930.8 eV appears which can be attributed to CuS. Similar transition to metal sulfide also has been reported for In_2O_3 gas sensor [157].

4.2. MOS modified with noble metal NPs

Noble metal NPs (Au, Ag, Pd, and Pt) not only can remarkably enhance the sensitivity, shorten the response/recovery times and enhance the selectivity, but also can decrease the operation temperature of gas sensor. Because at RT, the detection of a few gases like CO and H_2 by pristine MOS sensor is difficult. But, this issue can be solved by modifying the surface of the sensor using these noble metal NPs. Hence, the noble metal functionalization is regarded as one of the best approaches for enhancing gas sensing properties [78,158]. For example, Arunkumar et al. [159] prepared ZnO nanostars using a hydrothermal followed by the decoration of different wt% of Au NPS (as shown in Fig. 15(a–b).) The ZnO nanostars with 3 wt% Au NPs showed highest

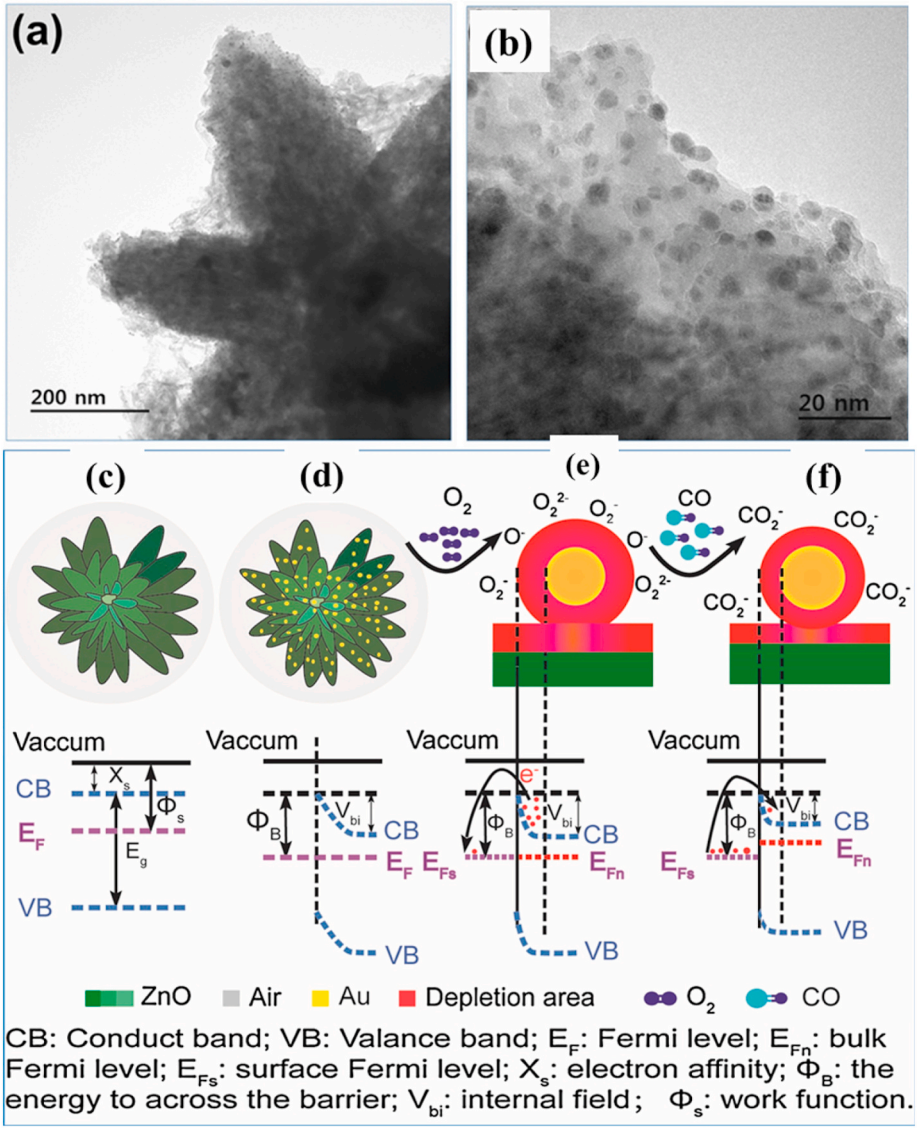

Fig. 15. (a–b) TEM images of 3 wt% Au loaded ZnO nanostars, and representative energy band diagram of pristine and Au loaded ZnO nanostars before (c–d) and after CO exposure (e–f). Reproduced from the ref 159, with the permission from Elsevier, copyright 2020.

surface area among other morphologies such as ZnO nanoflowers, marigold and nanorods. The Au-ZnO nanostars also exhibited excellent sensitivity (R_s = 35) towards 500 ppm CO with a very fast response/recovery times (41 s/40 s) at RT and excellent selectivity to CO among other interfering gases. Due to the spillover effect [160] of Au NPs, the thickness of EDL formed at the interface between Au and ZnO increases (Fig. 15(c–f)) and upon exposure to CO gas, significant reduction in the thickness of EDL, contributing to the sensing signal. Moreover, the hierarchical structure with numerous channels provided plenty of adsorption sites for CO gas molecules [161].

4.3. p-n heterojunction nanostructures

Composite structures comprising of n-p heterojunctions are highly demanded in gas sensing application due to their synergistic effects [84,94]. The sensing performance can be greatly improved due to the electronic sensitization at p-n heterojunctions and broadening of EDL on the interfaces between the sensing materials (Fig. 16(a)).

An ethanol sensor based on p-n NiO/SnO_2 nanocomposite reported recently [139]. The sensor exhibited a high sensitivity of (R_a/R_g=140) to 100 ppm ethanol at RT with fast response/recovery times of 23 and 13 s, respectively. The enhanced ethanol gas sensing was attributed to the formation of depletion layer at the p-n junction and catalytic activity of the NiO [140].

Another p-n heterojunction sensor was prepared by an electrospinning method using mesoporous In_2O_3-CuO composite nanofibers (Fig. 16(b)–(c)), with a high surface area of 48.7 m^2/g. Due to a mesoporous morphology and high surface area, as well as formation of p-n heterojunction (Fig. 16(d)), the sensor showed a response 1.5–100 ppm NH_3 at RT with good selectivity and fast dynamics [141].

4.4. MOS structure modified with 2D materials

Recently, various 2D nanomaterials, such as graphene and its derivatives, transition-metal dichalcogenides (TMDs), black phosphorous and transition-metal carbides/nitrides (MXene), have been used for the fabrication of RT gas sensors [145]. However, their RT sensing properties need to be enhanced in terms of sensitivity, selectivity and response/recovery [93,146,163,164]. The combination of these 2D materials with a MOS structure has led to significant improvements in the sensing properties [87].

Due to its excellent conductivity, high surface area, and unique 2D

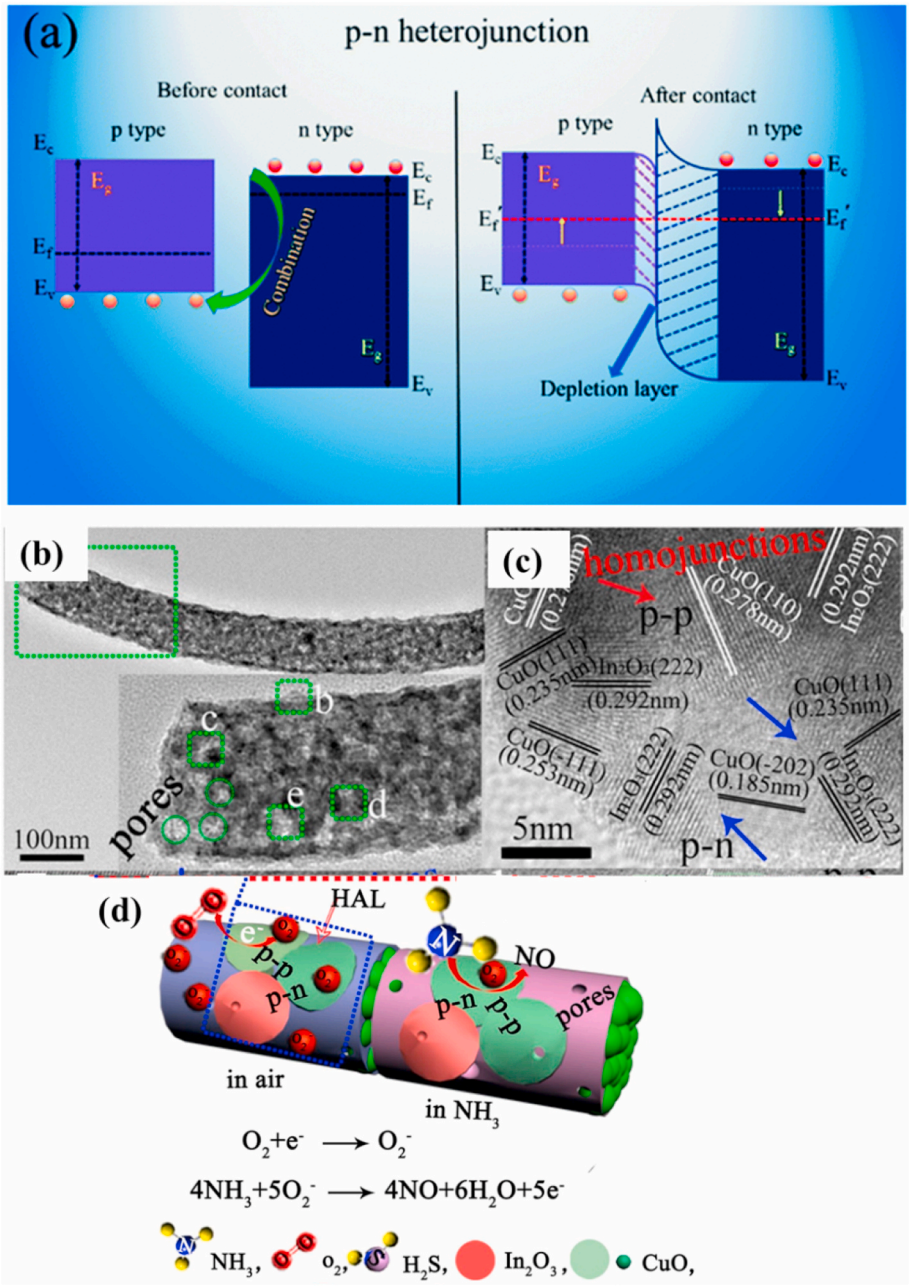

Fig. 16. (a) Schematic representation of the energy-band diagrams at heterojunction interfaces of different types of MOS heterojunctions. Reproduced from Ref [27] with the permission from Elsevier, Copyrights 2020. (b–c) TEM images of CuO-In_2O_3 composite nanofibers, and (d) Schematic of the sensing mechanism. Reproduced from Ref [141] with the permission from Elsevier, 2020.

structure, reduced graphene (rGO) has been recognized as a promising sensing material [165,166]. Especially, it is used in composite form to enhance its sensing properties. For example, a nanocomposite with a rGO-ZnO-SnO_2 heterostructure was synthesized by using the hydrothermal method [167]. The as-prepared ternary composite sensor exhibited a response ($\Delta R/R_a \times 100$) of 141% towards 5 ppm of NO_2 at RT. The presence of rGO led to rapid electron transfer between ZnO and SnO_2. Furthermore, the formation of p-n and n-n heterojunctions contributed to the enhanced NO_2 sensing characteristics.

In another study, Ma et al. reported RT gas-sensing three-dimensional (3D) Fe_3O_4-SiO_2-rGO core-shell spheres synthesized using electrostatic self-assembly, followed by thermal reduction [168]. The as-prepared 3D Fe_3O_4-SiO_2-rGO nanosphere suspensions (0.5 mg/mL) were dropped onto the sensor chip under a magnetic field (0.28 T) applied perpendicular to the electrodes, and after evaporation, the materials were aligned in the sensor electrodes to form uniform multi-channel sensing devices. The sensor exhibited an ultrahigh response of 34.41 toward 5 ppm of NO_2 at RT. The high sensing performance was related to the large sensing area resulting from the presence of rGO, to the 3D nature of the sensing layer, and to the high electron transport between rGO and Fe_3O_4-SiO_2.

Transition-metal dichalcogenides (TMDs) such as molybdenum disulfide (MoS_2) have grabbed tremendous attention due to their having high stability, numerous surface active sites for functionalization and gas adsorption, and good conductivity at RT [147,169]. However, the pristine MoS_2 gas sensors exhibit low sensitivity and slow dynamics at RT [170]. Accordingly, it is mostly used in a composite form. For example, Han et al. reported the fabrication of MoS_2/ZnO heterostructures via a wet chemical route [171]. The sensor showed a response ($\Delta I/I_a$) of 30.50 towards 5 ppm of NO_2 with an ultrafast response time

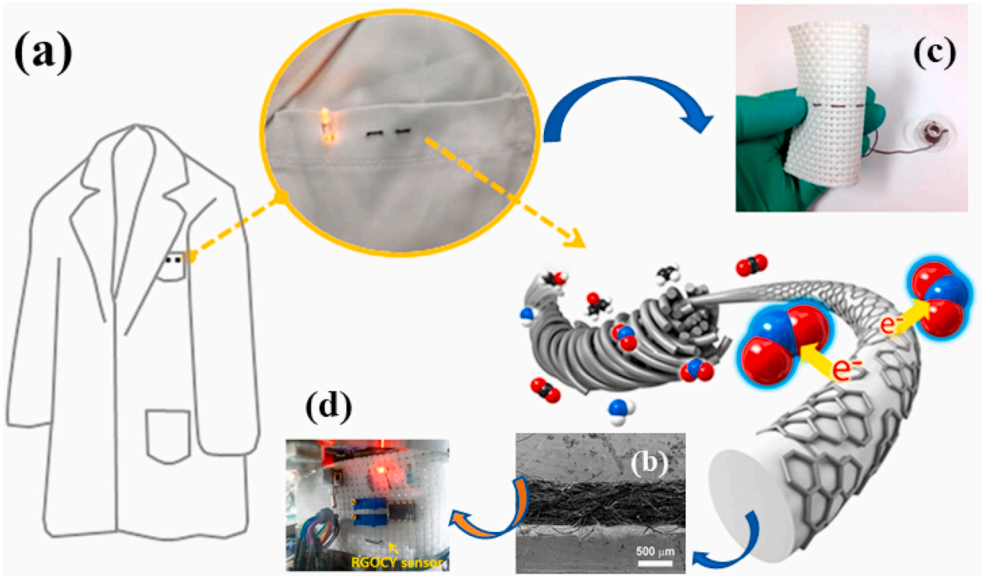

Fig. 17. (a)–(d) Wearable gas sensor based on RGOCY. Reproduced from Ref. 208 under the license of creative commons attribute (https://creativecommons.org/licenses/).

(40 s). The sensing mechanism was explained on the basis of the synergistic effects of the unique 2D/0D morphology and the formation of p-n junctions between ZnO and MoS_2 [172]. In another study related to MoS_2, Chen et al. reported the surface functionalization of MoS_2 by Au NPs for selective detection of acetone at RT [173]. The sensor exhibited high a response to acetone gas, which was related to the strong adsorption of acetone molecules on the Au-MoS_2 sensor and to the high catalytic activity of Au NPs towards acetone.

Another category of 2D materials with sheet-like or layered morphology is known as MXenes, which have a general formula of $Mn_{+1}AX_n$, (MAX phase), where M stands for a transition metal, A is a IIIA or IVA element, and X is N and/or C with n = 1, 2, or 3 [174–177]. The advantages of these materials are high conductivity, high surface area due to the unique 2D morphology, and excellent flexibility, which make them attractive materials for many applications, including gas sensing [176–179]. Some studies related to the gas-sensing properties of a pristine Mxene and its composites with a MOS structure have been published [179–183]. For example, Tai et al. designed an ammonia gas sensor made from $Ti_3C_2T_x$ and TiO_2 composite nanostructures [148]. TiO_2 NPs were deposited on the synthesized $Ti_3C_2T_x$ nanosheets to fabricate $TiO_2/Ti_3C_2T_x$ nanosheet composites. The fabricated gas sensor exhibited a higher response to ammonia relative to other gases at RT. The enhanced NH_3 sensing response of the sensor was explained using the model of self-built electric-field (space-charge layer) regulation. Upon intimate contact between $Ti_3C_2T_x$ and TiO_2, electrons in the conduction band of TiO_2 migrated to $Ti_3C_2T_x$ due to its excellent metallic properties and to the higher work function of $Ti_3C_2T_x$, leading to a self-built electric field (Schottky barrier) at their interface. In air, the density of holes on the surface of $Ti_3C_2T_x$ increases whereas the number of electrons on the surface of TiO_2 decreases because the electrons are consumed by the generated ionized adsorbed oxygen, resulting in a weakening of the self-built electric field due to the increased number of holes in $Ti_3C_2T_x$ and decreased resistance of $TiO_2/Ti_3C_2T_x$. On the contrary, in NH_3, the self-built electric field was strengthened due to a decrease in the number of holes on the surface of $Ti_3C_2T_x$ and an increase in the number of electrons on the surface of TiO_2 ($4NH_3 + 5O_2^- \rightarrow 4NO + 6H_2O + 5e^-$), leading to increased resistance.

4.5. MOS structure modified with conducting polymers

In addition to the MOS/rGO nanocomposites used for sensing studies [184–186], many MOS/conducting polymer (CP) composites have been used for such purposes. CPs such as polyaniline (PANI), polythiophene (PTh) and polypyrrole (PPy) are the most common polymers for RT gas-sensing studies due to their unique electrical and optical characteristics, low cost, ease of fabrication, and flexibility [187–189]. Most CPs have good sensitivity to ammonia gas, but in pristine form, their recovery times are long; thus, they are mostly used in composite form with MOS structures. For example, Beniwal et al. demonstrated NH_3 SnO_2/PPy electrospun composite sensors [190]. The sensor showed an excellent response ($\Delta R/R_a$) of 57% with a short response/recovery time of 18 s/30 s for 100 ppb of NH_3 at RT. The intrinsically good sensitivity of SnO_2 to NH_3, along with formation of p-n heterojunctions, led to the enhanced response to NH_3 at RT. Furthermore, PPy has a -NH- group, which can easily interact with NH_3 gas, thereby increasing the electrical resistance and, hence, the gas response. PPy/MnO_2 and PANI/Fe_2O_3 are other examples of composites used for RT gas-sensing studies [191,192]. Recently, a novel CuO-Chitosan nanocomposite H_2S gas sensor was introduced by Fajr et al. [189]. The sensor revealed a fast response of 14 s and a high response ($\Delta R/R_a$) of 217.89% for 100 ppm of H_2S gas at 40 °C. They also measured the power consumption of the sensor and found that it showed a power consumption of 0.45 W at 40 °C. The formation of heterojunctions and the catalytic effect of CuO contributed to the sensing signal.

4.6. MOS treated with UV-irradiation

A good strategy for decreasing the operation temperature of gas sensors is UV illumination. When the energy of UV light is equal or higher than the band gap energy of the sensing material, photogenerated electrons and holes can be produced by the absorption of UV light. In fact, the energy required to excite these electrons and holes is supplied by the light, instead of by heat. Furthermore, illumination facilitates the chemisorption of oxygen molecules on the surface to generate more O_2^- by improving the chemical activity of the surface [116] at RT as follows [150,160–162]:

$$h\nu \rightarrow h^+ + e^- \quad (12)$$

$$O_2 + e^- {}_{(h\nu)} \rightarrow O_2^-(h\nu) \rightarrow O_2^- {}_{(h\nu)}, \quad (13)$$

where ν is the frequency of the illuminated light and h is Planck's constant.

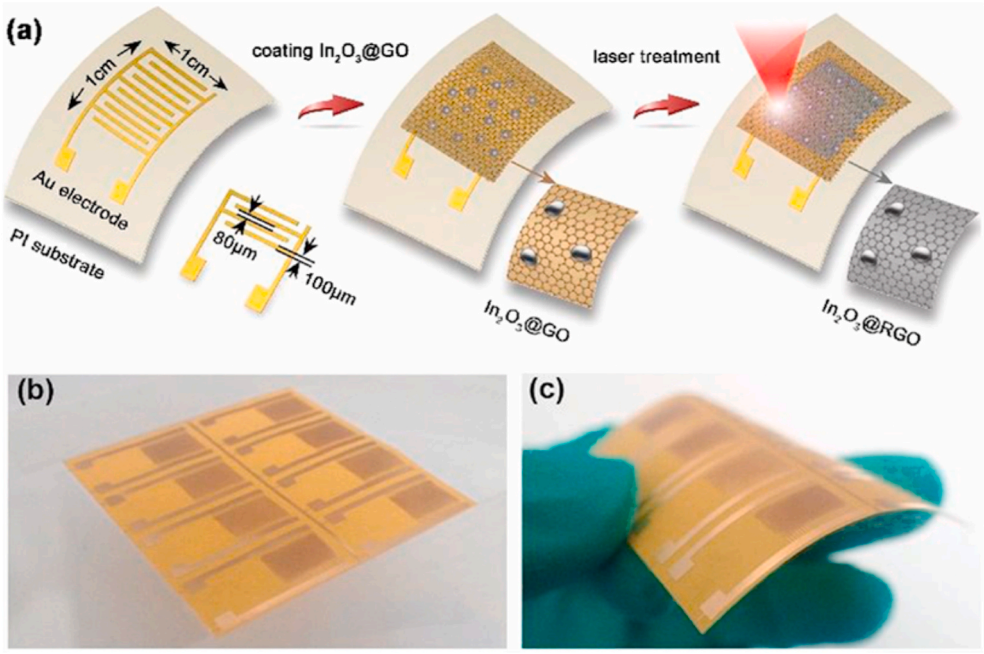

Fig. 18. (a) Schematic illustration for the fabrication of an In_2O_3-rGO film on a flexible PI substrate by using laser writing. (b, c) Photographs of the flexible PI. Reproduced from Ref 185 with permission from Elsevier, 2020.

Many reports about RT operation of gas sensors under UV illumination [117,193–195] have been published. For example, Cui et al. reported ZnO nanostructures with different morphologies (nanofibers, nanoflowers, nanoplates) for HCHO detection under illumination with UV light at RT [196]. The ZnO morphology played a significant role in the sensing capacity, and the ZnO nanofiber sensor was found to display a high response of 12.61 (I_g/I_a) to 100 ppm of HCHO under illumination with 365-nm UV light at RT. Initially, under exposure to UV light, chemisorbed oxygen ions are formed due to the removal of electrons from the conduction band of ZnO, resulting in the formation of a depletion layer. The photo-induced oxygen O_2^- ions ($h\nu$) are weakly bound to ZnO and can be removed just by turning-off the UV light. When a ZnO sensor is exposed to HCHO, the following reaction occurs:

$$O_2^- (h\nu) + HCHO_{(g)} \rightarrow CO_2 + H_2O + e^- . \quad (14)$$

The release of electrons and the desorption of oxygen species lead to a reduction in the thickness of the depletion layer and a decrease in the electrical resistance [196]. The sensing enhancement in ZnO nanofibers was related to the surface area (9.61 m^2/g) of this sensor with a fibrous structure being larger relative to those of other morphologies.

In this section, we discussed various strategies to enhance the RT sensing properties of MOS-based gas sensors. In general, different strategies such as composite made using n-n MOSs or p-n MOSs, decoration with noble-metal NPs, and morphology engineering, as well as hybrid composites with carbon materials or CPs, have been used to realize RT gas sensors. Gas sensor operating at low temperatures with little or no power consumption can be used for different applications. In the next section, we will discuss the most important applications of gas sensors , namely, flexible and wearable gas sensors.

5. Applications of low or RT gas sensors

5.1. Flexible and wearable sensors

Considering the types of substrates used for gas sensor fabrication, gas sensors can be divided into flexible and non-flexible (rigid) gas sensors. The non-flexible sensors, which are currently the most common types, are fabricated on rigid substrates. However, they are rigid and cannot be used in applications that require high flexibility. For example, in some applications such as personal use, a gas sensor must be flexible under mechanical deformations and must have properties making it suitable for wearing. Flexible gas sensors are realized on flexible substrates, and upon stretching, titling or bending, their properties should not change significantly [197]. Flexible gas sensors with low weight, low price, high flexibility, high stretchability, and high conformability can act as good platforms for wearable gas sensors and has significance in monitoring in ambient atmosphere at RT [198–200]. Wearable sensors with integrated wireless technology can be integrated to an end-user with the Internet of Things (IoT) and offer real-time information for personal use [201], which has opened a new path for smart wearable devices. Different flexible substrates, such as polyethylene-terephthalate (PET) [202], polyimide (PI) [203,204], Kapton® [205], have been used for the realization of flexible and wearable sensors. Graphene and its derivatives have been shown to be ideal candidates for flexible gas sensors due to their high mechanical strength, good stability, high carrier mobility, and good flexibility [206,207]. Moreover, gas sensors based on fibers or textiles have been investigated due to their potential applications in wearable devices. For example, Yun et al. reported a bendable and washable electronic-textile (*e*-textile) gas sensor based on a composite of RGO-decorated cotton yarn, the so-called RGOCY (Fig. 17 (a)) [208]. The sensor was able to sense NO_2 gas at RT. Fig. 17(b)–(e) show the performance of the fabricated gas sensor under different conditions, such as bending (bend radius of 1.0 mm) and straightening; even after washing with a detergent, the sensor showed stable sensing properties, demonstrating its excellent performance under different conditions. Moreover, after 1000 bending-straightening cycles, the sensor exhibited stable electrical and sensing properties. The stability under washing was attributed to the chemical against water and detergent and to the mechanical resistance to shearing resulting from friction between the yarn and the magnetic stirrer during the washing of the gas sensor.

Lee et al. first introduced a flexible hybrid sensor based on graphene fibers and $Ti_3C_2T_x$ Mxene fabricated by using a wet spinning process [150]. Initially, $Ti_3C_2T_x$ MXene was synthesized, after which it was dispersed with a GO suspension to be drop casted onto the Si/SiO_2 substrate to realize a composite sensor. After thermal activation at

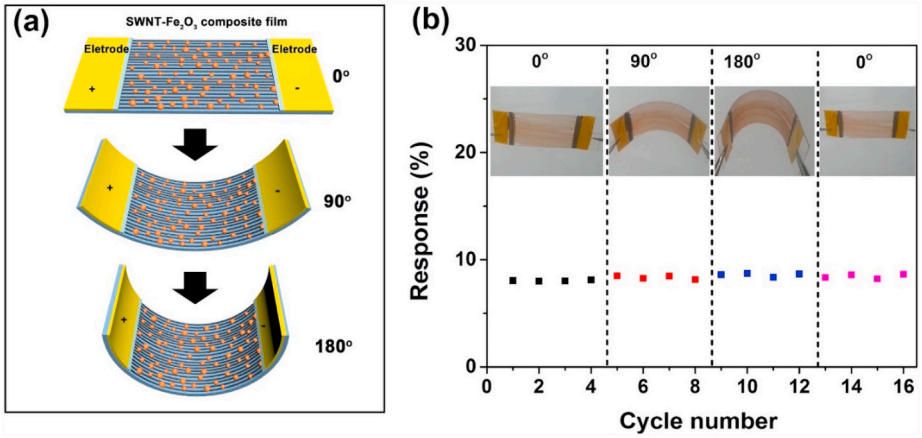

Fig. 19. (a) Schematic of a flexible SWNT-Fe_2O_3 sensor bent from 0° to 180°. (b) Response of a SWNT-Fe_2O_3 composite sensor to 20-ppm H_2S at different bending angles from 0° to 90°–180° to 0°. Reproduced from Ref. 212 with permission from Elsevier (Copyright 2020).

Table 2
Gas-sensing properties of RT-based gas sensors.

Sensing materials	Target gas/concentration	Response time/recovery time	Response [R_a/R_g or R_g/R_a] or *[(R_a-R_g/R_a) × 100]	Ref.
WO_3 hollow spheres	NO_2 (0.3 ppm)	670 s/2940 s	15.1	[152]
CuO nanosheets	H_2 S (0.01 ppm)	234 s/76 s	1.25	[135]
Au loaded ZnO nanostars	CO (500 ppm)	41 s-/40 s	55.3	[160]
Pt-PdO NWs	H_2 (10 ppm)	166 s	62%*	[163]
NiO-SnO_2 nanocomposites	C_2H_5OH (100 ppm)	23 s/13 s	140	[139]
In_2O_3-CuO composite nanofibers	NH_3 (100 ppm)	2 s/-	1.57	[141]
ZnO/SnO_2-rGO nanocomposite	NO_2 (5 ppm)	32 s/92 s	141%*	[167]
Fe_3O_4@SiO@rGO nanospheres	NO_2 1 ppm	250s/–	429%	[168]
MoS_2/ZnO p-n heterojunction	NO_2 (5 ppm)	40 s/–	30.5%	[172]
Au-loaded MOS_2	Acetone (120 ppm)	105 s/160 s	42.2%	[173]
TiO_2/$Ti_3C_2T_x$ Mxene composite	NH_3 (10 ppm)	33 s/277 s	3.1%	[148]
SnO_2/PPy nanofibers	NH_3 (0.1 ppm)	18 s/30 s	57%	[190]
UV irradiated ZnO nanofibers	HCHO (365 nm UV light)	–	12.61	[73]
rGO/$Ti_3C_2T_x$ Flexible composite	NH_3 (100 ppm)	4.2 min/13.3 min	6.7%	[150]
In_2O_3/rGO composite	NO_2 (1 ppm)	–	31.6%	[185]
PEDOT:PSS/rGO nanocomposite	(NH_3) 1000 ppm	–	18.9%	[209]
SWNT/Fe_2O_3 composite films	(NH_3) 200 ppm	250 s/350 s	4%	[212]

200 °C, the composite $Ti_3C_2T_x$/GO was reduced to $Ti_3C_2T_x$/rGO, and its gas-sensing properties at RT were measured. The sensor displayed an enhanced response to NH_3 ($\Delta R/R_0 \times 100 = 6.77\%$) with excellent flexibility and stability, enabling its use in portable and wearable sensing devices. At RT, the band gap of the $Ti_3C_2T_x$/rGO composite was widened from 1.05 eV to 1.57 eV, which had a positive effect on its sensing properties. Also, the optimum content of $Ti_3C_2T_x$ in the $Ti_3C_2T_x$/rGO composite was 40 wt%. For higher amounts of $Ti_3C_2T_x$, the band gap decreased, leading to a weak gas response due to the simultaneous increase in the density of charge carriers.

Many reports on rGO composite gas sensors with good flexibility have been published [183,184]. You et al. reported a flexible sensing device made of a composite film of graphene and In_2O_3 for NO_2 sensing at RT [185]. They designed a direct laser writing (DLW) process to integrate the In_2O_3-RGO sensor. The coated In_2O_3-GO film on a flexible substrate was converted to In_2O_3-RGO by using a CO_2 laser and a programmable scanning procedure (Fig. 18 (a)-(c)). One of the benefits of laser treatment is that it makes the sensor conducting due to the photo reduction of GO. Even though the initial In_2O_3-GO film was an insulator with high resistance, after laser treatment it was conductive. Although the In_2O_3-RGO composite sensor showed a good sensitivity to NO_2 gas, its response and recovery times were ~ 4.2 min/~ 13.3 min to 500 ppb of NO_2 gas at RT, which limit its applications in real situations.

In addition to the composites made from rGO/MOS [185], rGO/Mxene [183] and rGO-cotton Yarn [208], CP-based composites [188,209] have also been studied for flexible, wearable sensors at RT. PEDOT:PSS is a conjugated polymer that is widely used for flexible and printed electronics due to its good electrical conductivity, high transparency, and good processability. Seekaew et al. demonstrated a flexible gas sensor based on a PEDOT-PSS/graphene nanocomposite [209]. Yamazoe et al. demonstrated a flexible gas sensor based on a PEDOT-PSS/graphene nanocomposite [78]. The sensing film was deposited on a flexible substrate by using ink-jet printing. The ink for ink-jet printing was prepared using a PEDOT:PSS and graphene solution. The sensor showed high selectivity to NH_3 at RT and exhibited a p-type conducting behavior. The increased NH_3 sensing response for increased bending was related to the swelling effect of the sensor, where NH_3 gas molecules diffused into the graphene-PEDOT-PSS layer [210]. The enhanced sensing properties of the sensor were related to the direct charge-transfer process between the graphene-PEDOT-PSS surface and the NH_3 molecules due to the improved interactions via π electrons, the high specific surface area due to the presence of graphene with a sheet-like morphology, and the swelling due to the diffusion of NH_3 molecules into the graphene/polymer chain matrix [211].

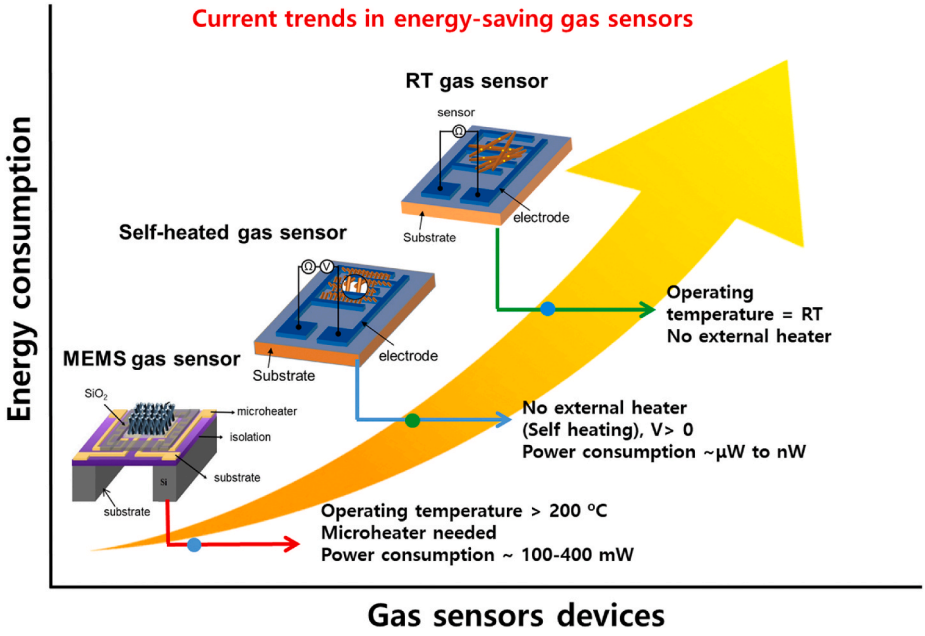

Scheme 1. An overview of resistive-based gas sensors based on their energy consumption point of view.

Other than the rGO, another carbon material, namely, a single wall carbon nanotube (SWCNT), has been utilized to realize flexible gas sensors due to its having a high surface area, porous structure, high conductivity, and strong affinity for the adsorbed gas molecules. For example, Hua et al. prepared SWNT-Fe_2O_3 composite films by combination of CVD and subsequent heat treatment in air [212]. As presented in Fig. 19(a), the gas sensor was deposited on a flexible plastic substrate, and it was able to be bent to large angles (90° and 180°) and then recover to its initial flat shape. The gas sensor's responses to 20 ppm of H_2S under different bending angles at RT are presented in Fig. 19(b). The sensor was deformed from a straight to a bent shape 16 times. Under all conditions, the sensor showed almost similar responses to H_2S gas.

RT gas sensors are in high demand for different applications because no external energy is required for their operation. Table 2 summarizes the RT gas-sensing properties of resistive-based gas sensors. The table clearly demonstrates that different sensing materials, whether in pristine, composite or decorated form, with various morphologies have been successfully used for RT gas sensors.

6. Conclusions, challenges and future perspectives

In this comprehensive review paper, we discussed the recent progress in the field of energy-saving gas sensors in terms of various sensing materials, sensing mechanisms, and strategies used to save energy. Due to the fast development of 5G technology and IoT and to further improvements of life service, in the near future, energy-saving gas sensors will be in high demand and will be extensively integrated into common electronic devices, such as smartphones, tablets, smart watches and so on. For these applications, realization of flexible, highly sensitive, selective, stable and cheap gas sensors with fast response and recovery times are in great demand.

Self-heating is a promising strategy for MOS-based gas sensors, especially for MOS materials with NW morphology. Operation of gas sensors in the self-heating mode can greatly decrease the power consumption from several µW to nW level. Such reductions in the power consumed can remarkably increase the sensor life and save a great amount of energy. Single, ordered, and networked NWs can be used for this purpose. However, synthesis of networked NWs is easier than that of single or ordered NWs, and as a result, currently, it is the most widely used morphology for self-heating gas sensors. However, mostly MOS materials with NW morphology have been reported for operation in self-heating mode. Thus, there is much room available for the future development of other morphology based self-heated gas sensors. Although, the self-heated gas sensors could able to show the power consumption in the range of nW level, however, the response value of most the sensors in this category are very less, which needed to be studied further.

Utilization of UV light is another technique used to decrease the operating temperature of gas sensors. UV light with energies higher than the band-gap energy of the sensing layer can excite electrons to the conduction band, and reactions of the electrons with oxygen and target gases can enhance the response of the sensor at RT. However, positioning a source of UV light just above the sensing layer is not always possible due to size limitations and economic considerations. Sensors that can work at RT without the need for UV light or operate in the self-heating mode do not need any external heater and, therefore, hold promise for energy-saving purposes. In addition to materials, morphology greatly affects the sensing properties of sensors that work at RT. Among different strategies to improve the gas-sensing properties of RT based gas sensors, the noble-metal functionalization and construction of heterojunction nanostructures are widely used. However, the operation of a sensor at RT has some challenges. The catalytic and sensitization effects are the main reasons for enhancement of sensitivity and selectivity of RT gas sensors. On the other hand, the synergistic effects of heterojunctions are the primary reason of the high sensing properties of p-n heterojunction based RT gas sensors. However, the humidity presence in the RT sensing ambient can significantly reduce the sensitivity of a gas sensor. Furthermore, most often the reactions cannot be completed at RT; accordingly, the response at RT is lower relative to those at higher temperatures.

MOS-based MEMS gas sensors are another choice as they have simple architectures, are easy to fabricate, and are efficient in term of energy use. In fact, the use of MEMS gas sensors not only can significantly decrease the final dimensions of the gas sensors but can also lead to reductions in power consumption in gas sensors and electronic devices. However, considering the power consumption of the above studied gas sensors, MEMS based gas sensor still behind the self-heated gas sensors (Scheme 1). One of the problems of MEMS gas sensors is they still use the external heater and gas sensing measurement still requires the elevated temperatures for the operation. Hence, it is still challenging to overcome

the issue. However, in case of RT based gas sensors, there are a few reports have been reported on the power consumption study. Despite of significant advances made so far in the developing low power consumption based gas sensors, several challenges and issues should be focused towards achieving high sensitivity, selectivity long-term stability with quick response/recovery time. In the future, with further developments of synthesis techniques, novel materials and creative technologies, high-performance gas sensors with high flexibility that can work at RT will be more readily available.

Declaration of competing interest

The authors declare that they have no known competing financial interests or personal relationships that could have appeared to influence the work reported in this paper.

Acknowledgements

This study was supported by the Basic Science Research Program of the National Research Foundation (NRF) of Korea funded by the Ministry of Education (2016R1A6A1A03013422), by the Korean government's Ministry of Science and ICT (MSIT) (2019R1A2C1006193), by the Ministry of Education, Science and Technology (2019R1A2B5B03069968), and by the Basic Science Research Program through the National Research Foundation of Korea (NRF) funded by the Korean Ministry of Science and ICT (MSIT) (2018R1A5A7025522).

Appendix A. Supplementary data

Supplementary data to this article can be found online at https://doi.org/10.1016/j.nanoen.2020.105369.

References

[1] G.F. Fine, L.M. Cavana, A. Afonja, R. Binions, Metal oxide semi-conductor gas sensors in environmental monitoring, Sensors 10 (2010) 5469–5502.
[2] D.J. Wales, J. Grand, V.P. Ting, R.D. Burke, K.J. Edler, C.R. Bowen, S. Mintova, A. D. Burrows, Gas sensing using porous materials for automotive applications, Chem. Soc. Rev. 44 (2015) 4290–4321.
[3] M.R. Miller, Oxidative stress and the cardiovascular effects of air pollution, Free Radic. Biol. Med. 151 (2020) 69–87.
[4] D.E. Schraufnagel, J.R. Balmes, C.T. Cowl, S. De Matteis, S.-H. Jung, K. Mortimer, R. Perez-Padilla, M.B. Rice, H. Riojas-Rodriguez, A. Sood, G.D. Thurston, T. To, A. Vanker, D.J. Wuebbles, Air pollution and noncommunicable diseases: a review by the forum of international respiratory societies' environmental committee, Chest 155 (2019) 417–426.
[5] D.A. Glencross, T.R. Ho, N. Camina, C.M. Hawrylowicz, P.E. Pfeffer, Air pollution and its effects on the immune system, Free Radic. Biol. Med. 151 (2020) 56–68.
[6] S. Mahajan, S. Jagtap, Metal-oxide semiconductors for carbon monoxide (CO) gas sensing: a review, Appl. Mater. Today 18 (2020), 100483.
[7] Z. Zhang, T. Xue, X. Jin, Effects of meteorological conditions and air pollution on COVID-19 transmission: evidence from 219 Chinese cities, Sci. Total Environ. 741 (2020), 140244.
[8] P. Kumar, A. Deep, K.-H. Kim, R.J.C. Brown, Coordination polymers: opportunities and challenges for monitoring volatile organic compounds, Prog. Polym. Sci. 45 (2015) 102–118.
[9] A. Mirzaei, S.G. Leonardi, G. Neri, Detection of hazardous volatile organic compounds (VOCs) by metal oxide nanostructures-based gas sensors: a review, Ceram. Int. 42 (2016) 15119–15141.
[10] Q. Ren, Y.Q. Cao, D. Arulraj, C. Liu, D. Wu, W.M. Li, A.D. Li, Review-resistive-type hydrogen sensors on zinc oxide nanostructures, J. Electrochem. Soc. 167 (2020), 067528.
[11] S. Nath, A. Dey, P. Pachal, J.K. Sing, S.K. Sarkar, Performance analysis of gas sensing device and corresponding IoT framework in mines, Microsys. Technol. (2019) 1–9.
[12] D.W. Kimmel, G. LeBlanc, M.E. Meschievitz, D.E. Cliffel, Electrochemical sensors and biosensors, Anal. Chem. 84 (2012) 685–707.
[13] K.-J. Kim, P. Lu, J.T. Culp, P.R. Ohodnicki, Metal-organic framework thin film coated optical fiber sensors: a novel waveguide based chemical sensing platform, ACS Sens. 3 (2018) 386–394.
[14] K.N. Chappanda, O. Shekhah, O. Yassine, S.P. Patole, M. Eddaoudi, K.N. Salama, The quest for highly sensitive QCM humidity sensors: the coating of CNT/MOF composite sensing films as case study, Sens. Actuators, B: Chem. 257 (2018) 609–619.
[15] S.G. Surya, S. Bhanoth, S.M. Majhi, Y.D. More, V.M. Teja, K.N. Chappanda, A silver nanoparticle-anchored UiO-66 (Zr) metal-organic framework (MOF)-based capacitive gas sensor, CrystEngComm 21 (2019) 7303–7312.
[16] S. Yuvraja, S.G. Surya, V. Chernikova, M.T. Vejjapu, O. Shekhah, P.M. Bhatt, S. Chandra, M. Eddaoudi, K.N. Salama, Realization of an ultrasensitive and highly selective OFET NO_2 Sensor: the synergistic combination of PDVT-10 polymer and porphyrin-MOF, ACS Appl. Mater. Interfaces 12 (2020) 18748–18760.
[17] K.S.N. Yamazoe, New perspectives of gas sensor technology, Sens. Actuators, B: Chem. 138 (2009) 100–107.
[18] R. Jaaniso, O.K. Tan, Semiconductor Gas Sensors, Woodhead Publishing Limited, Cambridge, UK, 2013.
[19] G. Korotcenkov, Metal oxides for solid-state gas sensors: what determines our choice? Mater. Sci. Eng. B 139 (2007) 1–23.
[20] D.R. Miller, S.A. Akbar, P.A. Morris, Nanoscale metal oxide-based heterojunctions for gas sensing: a review, Sens. Actuator B: Chem. 204 (2014) 250–272.
[21] M.M. Arafat, B. Dinan, S.A. Akbar, A.S.M.A. Haseeb, Gas sensors based on one dimensional nanostructured metal-oxides: a review, Sensors 12 (2012) 7207–7258.
[22] P. Srinivasan, M. Ezhilan, A.J. Kulandaisamy, K.J. Babu, J.B. Rayappan, Room temperature chemiresistive gas sensors: challenges and strategies-a mini review, J. Mater. Sci. Mater. Electron. 30 (2019) 1–23.
[23] Z.U. Abideen, J.-H. Kim, J.-H. Lee, J.-Y. Kim, A. Mirzaei, H.W. Kim, S.S. Kim, Electrospun metal oxide composite nanofibers gas sensors: a review, J. Kor. Ceram. Soc. 54 (2017) 366–379.
[24] T. Lin, X. Lv, S. Li, Q. Wang, The morphologies of the semiconductor oxides and their gas-sensing properties, Sensors 17 (2017) 2779.
[25] C. Wang, L. Yin, L. Zhang, D. Xiang, R. Gao, Metal oxide gas sensors: sensitivity and influencing factors, Sensors 10 (2010) 2088–2106.
[26] V. Dobrokhotov, A. Larin, D. Sowell, Vapor trace recognition using a single nonspecific chemiresistors, Sensors 13 (2013) 9016–9028.
[27] R. Ahmad, S.M. Majhi, X.X. Zhang, T.M. Swager, K.N. Salama, Recent progress and perspectives of gas sensors based on vertically oriented ZnO nanomaterials, Adv. Colloid Interface Sci. 270 (2019) 1–27.
[28] A. Mirzaei, J.H. Lee, S.M. Majhi, M. Weber, M. Bechelany, H.W. Kim, S.S. Kim, Resistive gas sensors based on metal-oxide nanowires, J. Appl. Phys. 126 (2019), 241102.
[29] H.-J. Kim, J.-H. Lee, Highly sensitive and selective gas sensors using p-type oxide semiconductors: Overview, Sens. Actuators B. Chem. 192 (2014) 607–627.
[30] Q. Ren, Y.Q. Cao, D. Arulraj, C. Liu, D. Wu, W.M. Li, A.D. Li, Resistive-type hydrogen sensors based on zinc oxide nanostructures, J. Electrochem. Soc. 167 (2020), 067528.
[31] H. Du, W. Yang, W. Yi, Y. Sun, N. Yu, J. Wang, Oxygen-plasma-assisted enhanced acetone-sensing properties of ZnO nanofibers by electrospinning, ACS Appl. Mater. Interfaces 12 (2020) 23084–23093.
[32] G. Korotcenkov, B.K. Cho, Engineering approaches to improvement of conductometric gas sensor parameters. Part 2: Decrease of dissipated (consumable) power and improvement stability and reliability, Sens. Actuators, B: Chem. 198 (2014) 316–341.
[33] T.M. Ngoc, N.V. Duy, C.M. Hung, N.D. Hoa, H. Nguyen, M. Tonezzer, N.V. Hieu, Self-heated Ag-decorated SnO_2 nanowires with low power consumption used as a predictive virtual multisensor for H_2S-selective sensing, Anal. Chim. Acta 1069 (2019) 108–116.
[34] D. Liu, L. Lin, Q. Chen, H. Zhou, J. Wu, Low power consumption gas sensor created from silicon nanowires/TiO_2 core-shell heterojunctions, ACS Sens. 2 (2017) 1491–1497.
[35] J. Lee, J. Kim, J.P. Im, S.Y. Lim, J.Y. Kwon, S.M. Lee, S.E. Moon, MEMS-based NO_2 gas sensor using ZnO nano-rods for low-power IoT application, J. Kor. Phys. Soc. 70 (2017) 924–928.
[36] D. Kohl, Function and application of gas sensors, J. Phys. D Appl. Phys. 34 (2001) R125–R149.
[37] X. Xue, Y. Nie, B. He, L. Xing, Y. Zhang, Z.L. Wang, Surface free-carrier screening effect on the output of a ZnO nanowire nanogenerator and its potential as a self-powered active gas sensor, Nanotechnology 24 (2013), 225501.
[38] T.M. Ngoc, N.V. Duy, C.M. Hung, N.D. Hoa, N.N. Trung, H. Nguyen, N.V. Hieu, Ultralow power consumption gas sensor based on a self-heated nanojunction of SnO_2 nanowires, RSC Adv. 8 (2018) 36323–36330.
[39] O. Monereo, O. Casals, J.D. Prades, A. Cirera, A low-cost approach to low-power gas sensors based on self-heating effects in large arrays of nanostructures, Procedia Eng. 120 (2015) 787–790.
[40] I. Cho, Y.C. Sim, M. Cho, Y.H. Cho, I. Park, Monolithic micro light-emitting diode/metal oxide nanowire sensor with microwatt-level power consumption, ACS Sens. 5 (2020) 563–570.
[41] A. Mirzaei, K. Janghorban, B. Hashemi, G. Neri, Metal-core@metal oxide-shell nanomaterials for gas-sensing applications: a review, J. Nanoparticle Res. 17 (2015) 371.
[42] S. Park, G.-J. Sun, H.J. Kheel, W.I. Lee, S. Lee, S.B.C. Lee, Synergistic effects of co-decoration of oxide nanoparticles on the gas sensing performance of In_2O_3 nanorods, Sens. Actuator, B: Chem. 227 (2016) 591–599.
[43] H.M. Tan, C.M. Hung, T.M. Ngoc, H. Nguyen, N.D. Hoa, N.V. Duy, N.V. Hieu, Novel self-heated gas sensors using on-chip networked nanowires with ultralow power consumption, ACS Appl. Mater. Interfaces 9 (2017) 6153–6162.
[44] A. Singh, A. Sharma, N. Dhul, A. Arora, M. Tomar, V. Gupta, MEMS based microheaters integrated gas sensors, Integr. Ferroelectr. 193 (2018) 72–78.
[45] Z. Wang, J. Song, Piezoelectric nanogenerators based on zinc oxide nanowire arrays, Science 312 (2006) 242–246.

[46] F. Fan, Z. Tian, Z. Wang, Flexible triboelectric generator, Nano Energy 1 (2012) 328–334.

[47] C. Wu, J.H. Park, B. Koo, X. Chen, Z.L. Wang, T.W. Kim, Capsule triboelectric nanogenerators: toward optional 3D integration for high output and efficient energy harvesting from broadband Amplitude vibrations, ACS Nano 12 (2018) 9947–9957.

[48] F. Yang, J. Guo, L. Zhao, W. Shang, Y. Gao, S. Zhang, G. Gu, B. Zhang, P. Cui, G. Cheng, Z. Du, Tuning oxygen vacancies and improving UV sensing of ZnO nanowire by microplasma powered by a triboelectric nanogenerator, Nano Energy 67 (2020), 104210.

[49] Y. Su, G. Xie, H. Tai, S. Li, B. Yang, S. Wang, Q. Zhang, H. Du, H. Zhang, X. Du, Y. Jiang, Self-powered room temperature NO_2 detection driven by triboelectric nanogenerator under UV illumination, Nano Energy 47 (2018) 316–324.

[50] Y. Fu, Y. Zhao, P. Wang, L. Xing, X. Xue, High response and selectivity of a Cu-ZnO nanowire nanogenerator as a self-powered/active H_2S sensor, Phys. Chem. Chem. Phys. 17 (2015) 2121–2126.

[51] Y. Lin, P. Deng, Y. Nie, Y. Hu, L. Xing, Y. Zhang, X. Xue, Room-temperature self-powered ethanol sensing of a Pd/ZnO nanoarray nanogenerator driven by human finger movement, Nanoscale 6 (2014) 4604–4610.

[52] L. Xing, Y. Hu, P. Wang, Y. Zhao, Y. Nie, P. Deng, X. Xue, Realizing room-temperature self-powered ethanol sensing of Au/ZnO nanowire arrays by coupling the piezotronics effect of ZnO and the catalysis of noble metal, Appl. Phys. Lett. 104 (2014), 013109.

[53] Y.Y. Zhao, X. Lai, P. Deng, Y.X. Nie, Y. Zhang, L.L. Xing, X.Y. Xue, Pt/ZnO nanoarray nanogenerator as self-powered active gas sensor with linear ethanol sensing at room temperature, Nanotechnology 25 (2014), 115502.

[54] Y. Fu, W. Zang, P. Wang, L. Xing, X. Xue, Y. Zhang, Portable room-temperature self-powered/active H_2 sensor driven by human motion through piezoelectric screening effect, Nano Energy 8 (2014) 34–43.

[55] Z. Qu, Y. Fu, B. Yu, P. Deng, L. Xing, X. Xue, High and fast H_2S response of NiO/ZnO nanowire nanogenerator as a self-powered gas sensor, Sens. Actuators B 222 (2016) 78–86.

[56] W. Zang, Y. Nie, D. Zhu, P. Deng, L. Xing, X. Xue, Core-shell In_2O_3/ZnO nanoarray nanogenerator as a self-powered active gas sensor with high H_2S sensitivity and selectivity at room temperature, J. Phys. Chem. C 118 (2014) 9209–9216.

[57] H. Zhang, Y. Yang, Y. Su, J. Chen, C. Hu, Z. Wu, Y. Liu, C.P. Wong, Y. Bando, Z. L. Wang, Triboelectric nanogenerator as self-powered active sensors for detecting liquid/gaseous water/ethanol, Nano Energy 2 (2013) 693–701.

[58] J.H. Kim, J. Chun, J.W. Kim, W.J. Choi, J.M. Baik, Self-powered, room-temperature electronic nose based on triboelectrification and heterogeneous catalytic reaction, Adv. Funct. Mater. 25 (2015) 7049–7055.

[59] X. Xue, Y. Fu, Q. Wang, L. Xing, Y. Zhang, Outputting olfactory bionic electric impulse by PANI/PTFE/PANI sandwich nanostructures and their application as flexible, smelling electronic skin, Adv. Funct. Mater. 26 (2016) 3128–3138.

[60] A.S.M.I. Uddin, U. Yaqoob, G.S. Chung, Improving the working efficiency of a triboelectric nanogenerator by the semimetallic PEDOT: PSS hole transport layer and its application in self-powered active acetylene gas sensing, ACS Appl. Mater. Interfaces 8 (2016) 30079–30089.

[61] L.F. Zhu, J.C. She, J.Y. Luo, S.Z. Deng, J. Chen, X.W. Ji, N.S Xu, Self-heated hydrogen gas sensors based on Pt-coated $W_{18}O_{49}$ nanowire networks with high sensitivity, good selectivity and low power consumption, Sens. Actuators, B: Chem. 153 (2011) 354–360.

[62] C. Fàbrega, O. Casals, F. Hernández-Ramírez, J.D. Prades, A review on efficient self-heating in nanowire sensors: prospects for very-low power devices, Sens. Actuators, B: Chem. 256 (2018) 797–811.

[63] T.M. Ngoc, N.V. Duy, N.D. Hoa, C.M. Hung, H. Nguyen, N.V. Hieu, Effective design and fabrication of low-power-consumption self-heated SnO_2 nanowire sensors for reducing gases, Sens. Actuators, B: Chem. 295 (2019) 144–152.

[64] A. Salehi, A highly sensitive self-heated SnO_2 carbon monoxide sensor, Sens. Actuators, B: Chem. 96 (2003) 88–93.

[65] C.Y. Lee, C.M. Chiang, Y.H. Wang, R.H. Ma, A self-heating gas sensor with integrated NiO thin-film for formaldehyde detection, Sens. Actuators, B: Chem. 122 (2007) 503–510.

[66] J.D. Prades, R. Jimenez-Diaz, F. Hernandez-Ramirez, S. Barth, Cirera, A. Romano-Rodriguez, S. Mathur, J. R. Morante, Ultralow power consumption gas sensors based on self-heated individual nanowires, Appl. Phys. Lett. 93 (2008), 123110.

[67] E. Strelcov, S. Dmitriev, B. Button, J. Cothren, V. Sysoev, A. Kolmakov, Evidence of the self-heating effect on surface reactivity and gas sensing of metal oxide nanowire chemiresistors, Nanotechnology 19 (2008), 355502.

[68] N.D. Chinh, N.V. Toan, V.V. Quang, N. Van Duy, N.D. Hoa, N.V. Hieu, Comparative NO_2 gas-sensing performance of the self-heated individual, multiple and networked SnO_2 nanowire sensors fabricated by a simple process, Sens. Actuators, B. Chem. 201 (2014) 7–12.

[69] P. Offermans, H.D. Tong, C.J.M. van Rijn, P. Merken, S.H. Brongersma, M. Crego-Calama, Ultralow-power hydrogen sensing with single palladium nanowires, Appl. Phys. Lett. 94 (22) (2009), 223110.

[70] D. Prades, F. Hernández-Ramírez, T. Fischer, M. Hoffmann, R. Müller, N. López, S. Mathur, J.R. Morante, Quantitative analysis of CO-humidity gas mixtures with self-heated nanowires operated in pulsed mode, Appl. Phys. Lett. 97 (24) (2010), 243105.

[71] J, Yun, C. Y.Jin, J.-H.Ahn, S.Jeon, I.Park, A self-heated silicon nanowire array: selective surface modification with catalytic nanoparticles by nanoscale Joule heating and its gas sensing applications, Nanoscale 5 (15) (2013) 6851–6856.

[72] G. Meng, F. Zhuge, K. Nagashima, A. Nakao, M. Kanai, Y. He, M. Boudot, T. Takahashi, K. Uchida, T. Yanagida, Nanoscale Thermal management of single SnO_2 nanowire: pico-Joule energy consumed molecule sensor, ACS Sens. 1 (2016) 997–1002.

[73] Y.-J. Choi, I.-S. Hwang, J.-G. Park, K.J. Choi, J.-H. Park, J.-H. Lee, Novel fabrication of and SnO_2 nanowire gas sensor with high sensitivity, ACS Appl. Mater. Interfaces 19 (2008), 95508.

[74] H.M. Tan, C.M. Hung, T.M. Ngoc, H. Nguyen, N.D. Hoa, N.V. Duy, N.V. Hieu, Novel self-heated gas sensors using on-chip networked nanowires with ultralow power consumption, ACS Appl. Mater. Interfaces 9 (2017) 6153–6162.

[75] V.V. Sysoev, J. Goschnick, T. Schneider, E. Strelcov, A. Kolmakov, A gradient microarray electronic nose based on percolating SnO_2 nanowire sensing elements, Nano Lett. 7 (10) (2007) 3182–3188.

[76] Y.J. Kwon, S.Y. Kang, P. Wu, Y. Peng, S.S. Kim, H.W. Kim, Selective improvement of NO_2 gas sensing behavior in SnO_2 nanowires by ion-beam irradiation, ACS Appl. Mater. Interfaces 8 (2016) 13646–13658.

[77] S. Zhou, M. Chen, Q. Lu, Y. Zhang, J. Zhang, B. Li, H.Wei, J. Hu, H. Wang Q. Liu, Zhou, Ag nanoparticles sensitized In_2O_3 nanograin for the ultrasensitive HCHO detection at room temperature, Nanoscale Res. Lett. 14 (2019) 365.

[78] N. Yamazoe, Y.Kurokawa, T. Seiyama Effects of additives on semiconductor gas sensors, Sensor. Actuator. B Chem. 4 (1983) 283–289.

[79] P.S. Kolhe, P.M. Koinkar, N. Maiti, K.M. Sonawane, Synthesis of Ag-doped SnO_2 thin films for the evaluation of H_2S gas sensing properties, Phys. B Condens. Matter. 524 (2017) 90–96.

[80] J. Gong, Q. Chen, M.-R. Lian, N.-C. Liu, R.G. Stevenson, F. Adami, Micromachined nanocrystalline silver doped SnO_2 H_2S sensor, Sensor. Actuator. B Chem. 114 (2006) 32–39.

[81] D.N. Chavan, G.E. Patil, D.D. Kajale, V.B. Gaikwad, P.K. Khanna, G.H. Jain, Nano Ag-doped In_2O_3 thick film: a low-temperature H_2S gas sensor, J. Sensors (2011) 1–8.

[82] J.-H. Kim, J.-H. Lee, Y. Park, J.-Y. Kim, A. Mirzaei, H.W. Kim, S.S. Kim, Toluene- and benzene-selective gas sensors based on Pt- and Pd-functionalized ZnO nanowires in self-heating mode, Sens. Actuators, B: Chem. 294 (2019) 78–88.

[83] J.-H. Kim, A. Mirzaei, H.W. Kim, S.S. Kim, Low power-consumption CO gas sensors based on Au-functionalized SnO_2-ZnO core-shell nanowires, Sens. Actuators, B: Chem. 267 (2018) 597–607.

[84] J.-H. Kim, H.W. Kim, S.S. Kim, Self-heating effects on the toluene sensing of Pt-functionalized SnO_2-ZnO core-shell nanowires, Sens. Actuators, B: Chem. 251 (2017) 781–794.

[85] J.H. Kim, A. Mirzaei, H.W. Kim, S.S. Kim, Pd-functionalized core-shell composite nanowires for self-heating, sensitive, and benzene-selective gas sensors, Sens. Actuators, A: Phys. 308 (2020), 112011.

[86] J.-Y. Kim, J.-H. Lee, J.-H. Kim, A. Mirzaei, H.W. Kim, S.S. Kim, Realization of H_2S sensing by Pd-functionalized networked CuO nanowires in self-heating mode, Sens. Actuators, B: Chem. 299 (2019), 126965.

[87] J.-H. Kim, A. Mirzaei, H.W. Kim, S.S. Kim, Realization of Au-decorated WS_2 nanosheets as low power-consumption and selective gas sensors, Sens. Actuators, B. Chem. 296 (2019), 126659.

[88] A. Katoch, J.-H. Byun, S.-W. Choi, S.S. Kim, One-pot synthesis of Au-loaded SnO_2 nanofibers and their gas sensing properties, Sensor. Actuator. B Chem. 202 (2014) 38–45.

[89] J.H. Lee, S. Kwak, J.H. Lee, I. Kim, Y.K. Yoo, T.H. Lee, Y.S. Shim, J. Kim, K.H. Lee, Sputtered PdO decorated TiO_2 sensing layer for a hydrogen gas sensor, J. Nanomater. (2018) 1–8.

[90] J.-H. Kim, A. Mirzaei, H.W. Kim, S.S. Kim, Extremely sensitive and selective sub ppm CO detection by the synergistic effect of Au nanoparticles and core-shell nanowires, Sensor. Actuator. B Chem. 249 (2017) 177–188.

[91] M.Z. Ansari, C. Cho, An analytical model of Joule heating in piezoresistive microcantilevers, Sensors 10 (2010) 9668–9686.

[92] O. Monereo, J.D. Prades, A. Cirera, Self-heating effects in large arrangements of randomly oriented carbon nanofibers: application to gas sensors, Sens. Actuators, B: Chem. 211 (2015) 489–497.

[93] J.M. Walker, S.A. Akbar, A.P. Morris, Synergistic effects in gas sensing semiconducting oxide nano heterostructures: a review, Sens. Actuators. B. Chem. 286 (2019) 624–640.

[94] D.R. Miller, S.A. Akbar, P.A. Morris, Nanoscale metal oxide-based heterojunctions for gas sensing: a review, Sensor. Actuator. B Chem. 204 (2014) 250–272.

[95] C. Balamurugan, G. Bhuvanalogini, A. Subramania, Development of nanocrystalline $CrNbO_4$ based p-type semiconducting gas sensor for LPG, ethanol and ammonia, Sensor. Actuator. B Chem. 168 (2012) 165–171.

[96] X. Xue, L. Xing, Y. Chen, S. Shi, Y. Wang, T. Wang, Synthesis and H_2S sensing properties of CuO-SnO_2 core/shell PN-junction nanorods, J. Phys. Chem. C 112 (2008) 12157–12160.

[97] S.-W. Choi, A. Katoch, J.-H. Kim, J.H. Lee, J.S. Lee, S.S. Kim, Importance of the nanograin size on the H_2S-sensing properties of ZnO-CuO composite nanofibers, Sensor. Actuator. B Chem. 214 (2015) 111–116.

[98] O. Monereo, S. Illera, A. Varea, M. Schmidt, T. Sauerwald, A. Schutze, A. Cirera, J.D. Prades, Localized self-heating in large arrays of 1D nanostructures, Nanoscale 8 (2016) 5082–5088.

[99] C.S. Prajapati, N. Bhatt, Self-heating oxidized suspended Pt nanowire for high performance hydrogen sensor, Sens. Actuators, B. Chem. 260 (2018) 236–242.

[100] K. Kalantar-zadeh, J.Z. Ou, T. Daeneke, M.S. Strano, M. Pumera, S.L. Gras, Two dimensional transition metal dichalcogenides in Biosystems, Adv. Funct. Mater. 25 (2015) 5086–5099.

[101] T. Xu, Y. Liu, Y. Pei, Y. Chen, Z. Jiang, Z. Shi, J. Xu, D. Wu, Y. Tian, X. Li, The ultrahigh NO_2 response of ultra-thin WS_2 nanosheets synthesized by hydrothermal and calcination processes, Sens. Actuators B. Chem. 259 (2018) 789–796.

[102] J. Seo, Y. Lim, H. Shin, Self-heating hydrogen gas sensor based on an array of single suspended carbon nanowires functionalized with palladium nanoparticles, Sens. Actuators, B. Chem. 247 (2017) 564–572.

[103] T.F. Choo, N.U. Saidin, K.Y. Kok, A novel self-heating zinc oxide/indium tin oxide-based hydrogen gas sensor: dual sensing mode of hydrogen gas detection, Chem. Phys. Lett. 713 (2018) 180–184.

[104] H.G. Moon, Y.S. Shim, H. Kim do, H.Y. Jeong, M. Jeong, J.Y. Jung, S.M. Han, J. K. Kim, J.S. Kim, H.H. Park, J.H. Lee, H.L. Tuller, S.J. Yoon, H.W. Jang, Self-activated ultra high chemosensitivity of oxide thin film nanostructures for transparent sensors, Sci. Rep. 2 (2012) 588.

[105] R.V. Gelato, F.P. Routinely, C. Verissimo, A.R. Vaz, M.A. Bica de Moraes, S. A. Moshkalev, Low-temperature gas and pressure sensor based on multi-wall carbon nanotubes decorated with Ti nanoparticles, Chem. Phys. Lett. 482 (2009) 302–306.

[106] J.-H. Ahn, J. Yun, D.-I. Moon, Y.-K. Choi, I. Park, Self-heated silicon nanowires for high performance hydrogen gas detection, Nanotechnology 26 (2015), 095501.

[107] J.Y. Seo, H.J. Shin, Self-heating hydrogen gas sensor based on an array of single suspended carbon nanowires functionalized with palladium nanoparticles, Sens. Actuators B 247 (2017) 564–572.

[108] K. Chikkadi, M. Muoth, V. Maiwald, C. Roman, C. Hierold, Ultra-low power operation of self-heated, suspended carbon nanotube gas sensors, Appl. Phys. Lett. 103 (2013), 223109.

[109] B. Ruhland, T. Becker, G. Müller, Gas-kinetic interactions of nitrous oxides with SnO_2 surfaces, Sens. Actuators, B: Chem. 50 (1998) 85–94.

[110] T.J. Hsueh, C.H. Peng, W.S. Chen, A transparent ZnO nanowire MEMS gas sensor prepared by an ITO micro-heater, Sens. Actuators, B: Chem. 304 (2020), 127319.

[111] J. Lee, J. Kim, P.J. Im, S.Y. Lim, J.Y. Kwon, S.M. Lee, S.E. Moon, MEMS-based NO_2 gas sensor using ZnO nano-rods for low-power IoT application, J. Kor. Phys. Soc. 70 (2017) 924–928.

[112] J. Burgués, S. Marco, Low power operation of temperature-modulated metal oxide semiconductor gas sensors, Sensors 18 (2018) 339.

[113] K.D. Mitzner, J. Sternhagen, D.W. Galipeau, Development of a micromachined hazardous gas sensor array, Sens. Actuators, B: Chem. 93 (2003) 92–99.

[114] L. Zhang, J. Zhao, H. Lu, L. Li, J. Zheng, H. Li, Z. Zhu, Facile synthesis and ultrahigh ethanol response of hierarchically porous ZnO nanosheets, Sens. Actuators, B: Chem. 161 (2012) 209–215.

[115] P. Ivanov, E. Llobet, X. Vilanova, J. Brezmes, J. Hubalek, X. Correig, Development of high sensitivity ethanol gas sensors based on Pt-doped SnO_2 surfaces, Sens. Actuators, B: Chem. 99 (2004) 201–206.

[116] S. Umesh, T.C. Balachandra, A. Usha, Design and simulation of MEMS gas sensor topologies for detection of inert gases, Mater. Today: Proc. 5 (2018) 21355–21362.

[117] R. Prajesh, N. Jain, V.K. Khanna, V. Gupta, A. Agarwal, MEMS based integrated gas sensor for NO_2 and NH_3, J. Inst. Smart Struc. Sys. (J. ISSS) 3 (2014) 1–6.

[118] H. Liu, L. Zhang, K.H.H. Li, O.K. Tan, Microhotplates for metal oxide semiconductor gas sensor applications-towards the CMOS-MEMS monolithic approach, Micromachines 9 (2018) 557.

[119] S.L. Firebaugh, K.F. Jensen, M.A. Schmidt, Investigation of high-temperature degradation of platinum thin films with an in-situ resistance measurement apparatus, J. Microelectromech. Sys 7 (1998) 128–135.

[120] S.S. Modal, S. Roy, C.K. Sarkar, Design and electrothermal analysis of MEMS based microheater array for gas sensor using INVAR alloy, 2012 International Conference on Communications, Devices and Intelligent Systems (CODIS), Kolkata, 2012, pp. 468–471.

[121] M.S. Haque, K.B.K. Teo, N.L. Rupensinghe, S.Z. Ali, I. Haneef, S. Maeng, J. Park, F. Udrea, W.I. Milne, On-chip deposition of carbon nanotubes using CMOS microhotplates, Nanotechnology 19 (2007), 025607.

[122] P. Bhattacharyya, Technological journey towards reliable microheater development for MEMS gas sensors: a review, IEEE Trans. Device Mater. Reliab. 14 (2014) 589–599.

[123] H.J. Pandya, S. Chandra, A.L. Vyas, Integration of ZnO nanostructures with MEMS for ethanol sensor, Sens. Actuators, B: Chem. 161 (2012) 923–928.

[124] R.E. Cavicchi, J.S. Suehle, K.G. Kreider, B.L. Shomaker, J.A. Small, M. Gaitan, P. Chaparala, Growth of SnO_2 films on micromachined hotplates, Appl. Phys. Lett. 66 (7) (1995) 812–814.

[125] P. Bhattacharyya, P.K. Basu, B. Mondal, H. Saha, A low power MEMS gas sensor based on nanocrystalline ZnO thin films for sensing methane, Microelectron. Reliab. 48 (2008) 1772–1779.

[126] S.E. Moon, H.K. Lee, N.J. Choi, J. Lee, C.A. Choi, W.S. Yang, J. Kim, J.J. Jong, D. J. Yoo, Low power consumption micro C_2H_5OH gas sensor based on micro-heater and screen printing technique, Sens. Actuators, B: Chem. 187 (2013) 598–603.

[127] T.J. Hsueh, C.H. Peng, W.S. Chen, A transparent ZnO nanowire MEMS gas sensor prepared by an ITO micro-heater, Sens. Actuators, B: Chem. 304 (2020), 127319.

[128] B. Behera, S. Chandra, An innovative gas sensor incorporating ZnO-CuO nanoflakes in planar MEMS technology, Sens. Actuators, B: Chem. 229 (2016) 414–424.

[129] K. Yuan, C.Y. Wang, L.Y. Zhu, Q. Cao, J.H. Yang, X.X. Li, W. Huang, Y.Y. Wang, H. L. Lu, D.W. Zhang, Fabrication of a micro-electromechanical system-based acetone gas sensor Using CeO_2 nanodot-decorated WO_3 nanowires, ACS Appl. Mater. Interfaces 12 (2020) 14095–14104.

[130] Y. Wang, C. Liu, Z. Wang, Z. Song, X. Zhou, N. Han, Y. Chen, Sputtered SnO_2: NiO thin films on self-assembled Au nanoparticle arrays for MEMS compatible NO_2 gas sensors, Sens. Actuators B: Chem. 278 (2019) 28–38.

[131] L. Siebert, N. Wolff, N. Ababii, M.-I. Terasa, O. Lupan, A. Vahl, V. Duppel, Haoyi Qiu, Maik Tienken, M. Mirabelli, V. Sontea, F. Faupel, L. Kienle, R. Adelung, Facile fabrication of semiconducting oxide nanostructures by direct ink writing of readily available metal microparticles and their application as low power acetone gas sensors, Nano Energy 70 (2020), 104420.

[132] Z. Li, H. Li, Z. Wu, M. Wang, J. Luo, H. Torun, P. Au, C. Yang, M. Grundmann, X. Lid, Y.Q. Fu, Advances in designs and mechanisms of semiconducting metal oxide nanostructures for high-precision gas sensors operated at room temperature, Mater. Horiz. 6 (2019) 470–506.

[133] T. Lin, X. Lv, Z. Hu, A. Xu, C. Feng, Semiconductor metal oxides as chemoresistive sensors for detecting volatile organic compounds, Sensors 19 (2019) 233.

[134] Z.S. Hosseini, A.I. Zad, A. Mortezaali, Room temperature H_2S gas sensor based on rather aligned ZnO nanorods with flower-like structures, Sens. Actuators, B: Chem. 207 (2015) 865–871.

[135] Z. Li, N. Wang, Z. Lin, J. Wang, W. Liu, K. Sun, Y.Q. Fu, Z. Wang, Room temperature high-performance H_2S sensor based on porous CuO nanosheets prepared by hydrothermal method, ACS Appl. Mater. Interfaces 8 (2016) 20962–20968.

[136] Jing Zhao,a Mengqing Hu,b Yan Liang,b Qiulin Li,b Xinye Zhangb, Zhenyu Wang, A room temperature sub-ppm NO_2 gas sensor based on WO_3 hollow spheres, New J. Chem. 44 (2020) 5064–5070.

[137] P. Jaroenapibal, P. Boonma, N. Saksilaporn, M. Horprathum, V. Amornkitbamrung, N. Triroj, Improved NO_2 sensing performance of electrospun WO_3 nanofibers with silver doping, Sens. Actuators, B 255 (2018) 1831–1840.

[138] O. Lupan, V. Postica, F. Labat, I. Ciofini, T. Pauporte, R. Adelung, Ultra-sensitive and selective hydrogen nanosensor with fast response at room temperature based on a single Pd/ZnO nanowire, Sens. Actuators, B: Chem. 254 (2018) 1259–1270.

[139] N. Jayababua, M. Polojua, J. Shruthia, M. Reddy, Semi shield driven p-n heterostructures and their role in enhancing the room temperature ethanol gas sensing performance of NiO/SnO_2 nanocomposites, Ceram. Int. 45 (2019), 15134.

[140] Z. Qu, Y. Fu, B. Yu, P. Deng, L. Xing, X. Xue, High and fast H_2S response of NiO/ZnO nanowire nanogenerator as a self-powered gas sensor, Sensor. Actuator. B Chem. 222 (2016) 78–86.

[141] J. Zhou, M. Ikram, A.U. Rehman, J. Wang, Y. Zhao, K. Kan, W. Zhang, F. Raziq, L. Li, K. Shi, Highly selective detection of NH_3 and H_2S using the pristine CuO and mesoporous In_2O_3@CuO multijunctions nanofibers at room temperature, Sens. Actuators, B 255 (2018) 1819–1830.

[142] E. Llobet, Gas sensors using carbon nanomaterials: a review, Sens. Actuators, B: Chem. 179 (2013) 32–45.

[143] Y.C. Wong, B.C. Ang, A.S.M.A. Haseeb, A.A. Baharuddin, Y.H. Wong, Conducting polymers as chemiresistive gas sensing materials: a review, J. Electrochem. Soc. 167 (2020), 037503.

[144] C. Wang, J. Zhu, S. Liang, H. Bi, Q. Han, X. Liu, X. Wang, Reduced graphene oxide decorated with CuO-ZnO hetero-junctions: towards high selective gas-sensing property to acetone, J. Mater. Chem. A 2 (2014) 18635–18643.

[145] X. Liu, T. Ma, N. Pinna, J. Zhang, Two-dimensional nanostructured materials for gas sensing, Adv. Funct. Mater. 27 (2017), 1702168.

[146] S. Gupta Chatterjee, S. Chatterjee, A.K. Ray, A.K. Chakraborty, Graphene-metal oxide nanohybrids for toxic gas sensor: a review, Sens. Actuators, B: Chem. 221 (2015) 1170–1181.

[147] B. Cho, J. Yoon, S.K. Lim, A.R. Kim, D.-H. Kim, S.-G. Park, J.-D. Kwon, Y.-J. Lee, K.-H. Lee, B.-H. Lee, H.-C. Ko, M.G. Hahm, Chemical sensing of 2D graphene/MoS_2 heterostructures device, ACS Appl. Mater. Interfaces 7 (2015) 16775–16780.

[148] H. Tai, Z. Duan, Z. He, X. Li, J. Xu, B. Liu, Y. Jiang, Enhanced ammonia response of $Ti_3C_2T_x$ nanosheets supported by TiO_2 nanoparticles at room temperature, Sens. Actuators B Chem. 298 (2019), 126874.

[149] E. Espid, F. Taghipour, UV-LED photo-activated chemical gas sensors: a review, Crit. Rev. Solid State Mater. Sci. 42 (2017) 416–432.

[150] H. Chen, Y. Liu, C. Xie, J. Wu, D. Zeng, Y. Liao, A comparative study on UV light activated porous TiO_2 and ZnO film sensors for gas sensing at room temperature, Ceram. Int. 38 (2012) 503–509.

[151] Z. Yuan, R. Li, F. Meng, J. Zhang, K. Zuo, E. Han, Approaches to enhancing gas sensing properties: a review, Sensors 19 (2019) 1495.

[152] J. Zhao, M. Hu, Y. Liang, Q. Li, X. Zhang, Z. Wang, A room temperature sub-ppm NO_2 gas sensor based on WO_3 hollow spheres, New J. Chem. 44 (2020) 5064–5070.

[153] Y. Song, F. Chen, Y. Zhang, S. Zhang, F. Liu, P. Sun, X. Yan, G. Lu, Fabrication of highly sensitive and selective room-temperature nitrogen dioxide sensors based on the zno nanoflowers, Sens. Actuators, B 287 (2019) 191–198.

[154] Z. Zhang, M. haq, Z. Wen, Z. Ye, L. Zhu, Ultrasensitive ppb-level NO_2 gas sensor based on WO_3 hollow nanospheres doped with Fe, Appl. Surf. Sci. 434 (2018) 891–897.

[155] G. Zhang, S. Zhang, L. Yang, Z. Zou, D. Zeng, C. Xie, La_2O_3-sensitized SnO_2 nanocrystalline porous film gas sensors and sensing mechanism toward formaldehyde, Sens. Actuators, B vol. 188 (2013) 137–146.

[156] Z. Li, J. Wang, N. Wang, S. Yan, W. Liu, Y.Q. Fu, Z. Wang, Hydrothermal synthesis of hierarchically flower-like CuO nanostructures with porous nanosheets for excellent H2S sensing, J. Alloys Compd. 725 (2017) 1136–1143.

[157] Vanish Kumar, Sanjit Manohar Majhi, Ki Hyun Kim, Hyoun Woo Kim, Eilhann E. Kwon, Advances in In_2O_3-based materials for the development of hydrogen sulfide Sensors, Chem. Eng. J. 404 (2021), 126472.

[158] P. Rai, S. M Majhi, Y. T Yu, J. H Lee, Noble metal@metal oxide semiconductor core@shell nano-architectures as a new platform for gas sensor applications, RSC Adv. 5 (2015) 76229–76248.

[159] S. Arunkumar, T. Hou, Y.-B. Kim, B. Choi, S.H. Park, S. Jung, D.-W. Lee, Au Decorated ZnO hierarchical architectures: facile synthesis, tunable morphology

and enhanced CO detection at room temperature, Sens. Actuators, B vol. 243 (2017) 990–1001.
[160] S.M. Majhi, P. Rai, Y. T Yu, Facile approach to synthesize Au@ZnO core-shell nanoparticles, and their application for highly sensitive and selective gas sensors, ACS Appl. Mater. Interfaces 7 (2015) 9462–9468.
[161] N. Singh, R.K. Gupta, P.S. Lee, Gold-nanoparticle-functionalized In_2O_3 nanowires as CO gas sensors with a significant enhancement in response, ACS Appl. Mater. Interfaces 3 (2011) 2246–2252.
[162] H.-J. Cho, V.T. Chen, S. Qiao, W.-T. Koo, R.M. Penner, I.-D. Kim, Pt-functionalized PdO nanowires for room temperature hydrogen gas sensors, ACS Sens. 3 (2018) 2152–2158.
[163] H. Li, J. Wu, Z. Yin, H. Zhang, Preparation and applications of mechanically exfoliated single-layer and multilayer MoS_2 and WSe_2 nanosheets, Acc. Chem. Res. 47 (2014) 1067–1075.
[164] D.J. Late, Y.-K. Huang, B. Liu, J. Acharya, S.N. Shirodkar, J. Luo, A. Yan, D. Charles, U.V. Waghmare, V.P. Dravid, C.N.R. Rao, Sensing behavior of atomically thin-layered MoS_2 transistors, ACS Nano 7 (2013) 4879–4891.
[165] Z. Chen, J. Wang, D. Pan, Y. Wang, R. Noetzel, H. Li, P. Xie, W. Pei, A. Umar, L. Jiang, Nan Li, N. F. de Rooij, G. Zhou, mimicking a dog's nose: scrolling graphene nanosheets, ACS Nano 12 (2018) 2521–2530.
[166] F. Rascha, V. Posticab, F. Schütta, Y.K. Mishra, A.S. Nia, M.R. Lohe, X. Feng, R. Adelung, O. Lupan, Highly selective and ultra-low power consumption metal oxide based hydrogen gas sensor employing graphene oxide as molecular sieve, Sens. Actuators: B Chem. 320 (2020) 2048–2057, 128363.
[167] Z. Wang, S. Gao, T. Fei, S. Liu, T. Zhang, Construction of ZnO SnO_2 heterostructure on reduced graphene oxide for enhanced nitrogen dioxide sensitive performances at room temperature, ACS Sens. 4 (8) (2019) 2048–2057.
[168] D. Ma, Y. Su, T. Tian, H. Yin, C. Zou, T. Huo, N. Hu, Z. Yang, Y. Zhang, Multichannel room-temperature gas sensors based on magnetic-field aligned 3D Fe_3O_4@SiO_2@Reduced graphene oxide spheres, ACS Appl. Mater. Interfaces 12 (3) (2020) 37418–37426.
[169] D. Zhang, J. Wu, P. Li, Y. Cao, Room-temperature SO_2 gas sensing properties based on a metal-doped MoS_2 nanoflower: an experimental and density functional theory investigation, J. Mater. Chem. 5 (2017) 20666–20677.
[170] K. Lee, R. Gatensby, N. McEvoy, T. Hallam, G.S. Duesberg, High-performance sensors based on molybdenum disulfide thin films, Adv. Mater. 25 (2013) 6699–6702.
[171] Y. Han, D. Huang, Y. Ma, G. He, J. Hu, J. Zhang, N. Hu, Y. Su, Z. Zhou, Y. Zhang, Z. Yang, Design of hetero-nanostructures on MoS_2 nanosheets to boost NO_2 room-temperature sensing, ACS Appl. Mater. Interfaces 10 (2018) 22640–22649.
[172] K. Xu, N. Li, D. Zeng, S. Tian, S. Zhang, D. Hu, C Xie, Interface bonds determined gas-sensing of SnO_2-SnS_2 hybrids to ammonia at room temperature, ACS Appl. Mater. Interfaces 7 (2015) 11359–11368.
[173] W.Y. Chen, C.-C. Yen, S. Xue, H. Wang, L.A. Stanciu, Surface functionalization of layered molybdenum disulfide for the selective detection of volatile organic compounds at Room Temperature, ACS Appl. Mater. Interfaces 11 (2019) 34135–34143.
[174] J. Zhu, E. Ha, G. Zhao, Y. Zhou, D. Huang, G. Yue, L. Hu, N. Sun, Y. Wang, L.Y. S. Lee, C. Xu, K.Y. Wong, D. Astruc, P. Zhao, Recent advance in MXenes: a promising 2D material for catalysis, sensor and chemical adsorption, Coord. Chem. Rev. 352 (2017) 306–327.
[175] M. Naguib, O. Mashtalir, J. Carle, V. Presser, J. Lu, L. Hultman, Y. Gogotsi, M. W. Barsoum, Two-dimensional transition metal carbides, ACS Nano 6 (2012) 1322–1331.
[176] M. Alhabeb, K. Maleski, B. Anasori, P. Lelyukh, L. Clark, S. Sin, Y. Gogotsi, Guidelines for synthesis and processing of two-dimensional titanium carbide ($Ti_3C_2T_x$ MXene), Chem. Mater. 29 (2017) 7633–7644.
[177] M. Naguib, V.N. Mochalin, M.W. Barsoum, Y. Gogotsi, 25th anniversary article: MXenes: a new family of two-dimensional materials. Advanced materials, Adv. Mater. 26 (2014) 992–1005.
[178] B. Anasori, M.R. Lukatskaya, Y. Gogotsi, 2D metal carbides and nitrides (MXenes) for energy storage, Nat. Rev. Mater. 2 (2017) 1–17.
[179] E. Lee, A. Vahid Mohammadi, B.C. Prorok, Y.S. Yoon, M. Beidaghi, D.-J. Kim, Room temperature gas-sensing of Two dimensional titanium carbide (MXene), ACS Appl. Mater. Interfaces 9 (2017) 37184–37190.
[180] S.J. Kim, H.-J. Koh, C.E. Ren, O. Kwon, K. Maleski, S.-Y. Cho, B. Anasori, C.-K. Kim, Y.-K. Choi, J. Kim, Y. Gogotsi, H.-T. Jung, Metallic $Ti_3C_2T_x$ MXene gas sensors with ultrahigh signal-to-noise ratio, ACS Nano 12 (2018) 986–993.
[181] W. Yuan, K. Yang, H. Peng, F. Li, F. Yin, A flexible VOCs sensor based on a 3D MXene framework with a high sensing performance, J. Mater. Chem. A 6 (2018) 18116–18124.
[182] E. Lee, A.V. Mohammadi, Y.S. Yoon, M. Beidaghi, D.-J. Kim, Two-dimensional vanadium carbide MXene for gas sensors with ultrahigh sensitivity toward nonpolar gases, ACS Sens. 4 (2019) 1603–1611.
[183] S.H. Lee, W. Eom, H.S. Shin, R.B. Ambade, J.H. Bang, H.W. Kim, T.H. Han, Room-Temperature, Highly Durable $Ti_3C_2T_x$ MXene/Graphene hybrid fibers for NH_3 gas sensing, ACS Appl. Mater. Interfaces 12 (2020) 10434–10442.
[184] Z. Xiao, L.B. Kong, S. Ruan, X. Li, S. Yu, X. Li, Y. Jiang, Z. Yao, S. Ye, C. Wang, T. Zhang, Recent development in nanocarbon materials for gas sensor applications, Sens. Actuators, B: Chem. 274 (2018) 235–267.
[185] R. You, D.D. Han, F. Liu, Y.L. Zhang, G. Lu, Fabrication of flexible room-temperature NO_2 sensors by direct laser writing of In_2O_3 and graphene oxide composites, Sens. Actuators, B: Chem. 277 (2018) 114–120.
[186] Y.L. Dong, X.F. Zhang, X.L. Cheng, Y.M. Xu, S. Gao, H. Zhao, L.H. Huo, Highly selective NO_2 sensor at room temperature based on nanocomposites of hierarchical nanosphere-like α-Fe_2O_3 and reduced graphene oxide, RSC Adv. 4 (2014) 57493–57500.
[187] H. Bai, G. Shi, Gas sensors based on conducting polymers, Sensors 7 (2007) 267–307.
[188] S. Abdulla, T.L. Mathew, B. Pullithadathil, Highly sensitive, room temperature gas sensor based on polyaniline-multiwalled carbon nanotubes (PANI/MWCNTs) nanocomposite for trace-level ammonia detection, Sens. Actuators, B: Chem. 221 (2015) 1523–1534.
[189] F.I.M. Alia, S.T. Mahmoud, F. Awwadb, Y.E. Greishc, A.F.S. Abu-Hani, Low power consumption and fast response H_2S gas sensor based on a chitosan-CuO hybrid nanocomposite thin film, Carbohydr. Polym. 236 (2020), 116064.
[190] A. Beniwal, Sunny, Electrospun SnO_2/PPy nanocomposite for ultra-low ammonia concentration detection at room temperature, Sens. Actuators B: Chem. 296 (2019), 126660.
[191] K. Malook, H. Khan, M. Shah, I. Haque, Highly selective and sensitive response of polypyrrole-MnO_2 based composites towards ammonia gas, Polym. Compos. 10 (2019) 1675.
[192] C. Zhu, U. Cakmak, O. Sheikhnejad, X. Cheng, X. Zhang, Y. Xu, S. Gao, H. Zhao, L. Huo, Z. Major, One step synthesis of PANI/Fe_2O_3 nanocomposites and flexible film for enhanced NH_3 sensing performance at room temperature, Nanotechnology 30 (2019), 255502.
[193] S. Fan, A. Srivastava, V. Dravid, UV-activated room-temperature gas sensing mechanism of polycrystalline ZnO, Appl. Phys. Lett. 95 (2009), 142106.
[194] C. Zhang, G. Liu, X. Geng, K. Wu, M. Debliquy, Metal oxide semiconductors with highly concentrated oxygen vacancies for gas sensing materials: a review, Sens. Actuators, A: Phys. 309 (2020), 112026.
[195] C. Zhang, A. Boudiba, P. Marco, R. Snyders, M. Olivier, M. Debliquy, Room temperature responses of visible-light illuminated WO_3 sensors to NO_2 in sub-ppm range, Sens. Actuators, B: Chem. 181 (2013) 395–401.
[196] J. Cui, L. Shi, T. Xie, D. Wang, Y. Lin, UV-light illumination room temperature HCHO gas-sensing mechanism of ZnO with different nanostructures, Sens. Actuators, B: Chem. 227 (2016) 220–226.
[197] A. Nag, S.C. Mukhopadhyay, J. Kosel, Wearable flexible sensors: a review, IEEE Sens. J. 17 (2017) 3949–3960.
[198] Y. Yang, W. Gao, Wearable and flexible electronics for continuous molecular monitoring, Chem. Soc. Rev. 48 (2019) 1465–1491.
[199] M. Mardonova, Y. Choi, Review of wearable device technology and its applications to the mining industry, Energies 11 (2018) 547.
[200] J. Park, J. Kim, K. Kim, S.-Y. Kim, W.H. Cheong, K. Park, J.H. Song, G. Namgoong, J.J. Kim, J. Heo, F. Bien, J.-U.Park, Wearable, wireless gas sensors using highly stretchable and transparent structures of nanowires and graphene, Nanoscale 8 (2016) 10591–10597.
[201] A. Pantelopoulos, N.G. Bourbakis, A survey on wearable sensor-based systems for health monitoring and prognosis, IEEE T. Syst. Man Cy. C 40 (2009) 1–12.
[202] Z.Q. Zheng, J.D. Yao, B. Wang, G.W. Yang, Light-controlling, flexible and transparent ethanol gas sensor based on ZnO nanoparticles for wearable devices, Sci. Rep. 5 (2015), 11070.
[203] Y.S. Kim, Microheater-integrated single gas sensor array chip fabricated on flexible polyimide substrate, Sens. Actuators, B: Chem. 114 (2006) 410–417.
[204] Z. Zheng, J. Yao, B. Wang, G. Yang, A flexible, transparent and high-performance gas sensor based on layer-materials for wearable technology, Nanotechnology vol. 28 (2017), 415501.
[205] P.M. Perillo, D.F. Rodríguez, Low temperature trimethylamine flexible gas sensor based on TiO_2 membrane nanotubes, J. Alloys Compd. 657 (2016) 765–769.
[206] E. Singh, M. Meyyappan, H.S. Nalwa, Flexible graphene-based wearable gas and chemical sensors, ACS Appl. Mater. Interfaces 9 (2017) 34544–34586.
[207] B. Cho, J. Yoon, M.G. Hahm, D.H. Kim, A.R. Kim, Y.H. Kahng, S.W. Park, Y.J. Lee, S.G. Park, J.D. Kwon, C.S. Kim, Graphene-based gas sensor: metal decoration effect and application to a flexible device, J. Mater. Chem. C 2 (2014) 5280–5285.
[208] Y.J. Yun, W.G. Hong, N.J. Choi, B.H. Kim, Y. Jun, H.K. Lee, Ultrasensitive and highly selective graphene-based single yarn for use in wearable gas sensor, Sci. Rep. 5 (2015), 10904.
[209] Y. Seekaew, S. Lokavee, D. Phokharatkul, A. Wisitsoraat, T. Kerdcharoen, C. Wongchoosuk, Low-cost and flexible printed graphene-PEDOT: PSS gas sensor for ammonia detection, Org. Electron. 15 (2014) 2971–2981.
[210] X. Crispin, S. Marciniak, W. Osikowicz, G. Zotti, A.W. Denier VanderGon, F. Louwet, M. Fahlman, L. Groenendaal, F. Deschryver, W.R. Salaneck, Conductivity, morphology, interfacial chemistry, and stability of poly(3,4-ethylene dioxythiophene)–poly(styrenesulfonate): a photoelectron spectroscopy study, J. Polym. Sci. B Polym. Phys. 41 (2003) 2525–2561.
[211] Z. Wu, X. Chen, S. Zhu, Z. Zhou, Y. Yao, W. Quan, B. Liu, Enhanced sensitivity of ammonia sensor using graphene/polyaniline nanocomposite, Sens. Actuators, B: Chem. 178 (2013) 485–493.
[212] C. Hua, Y. Shang, Y. Wang, J. Xu, Y. Zhang, X. Li, A. Cao, A flexible gas sensor based on single-walled carbon nanotube-Fe_2O_3 composite film, Appl. Surf. Sci. 405 (2017) 405–411.

Sanjit Manohar Majhi received his Ph.D. degree in August 2017 from Chonbuk National University, South Korea, and worked on the synthesis of noble metal nanoparticles and metal oxide semiconductors to design core@shell nanostructures for gas sensor applications. Then he was a Postdoctoral fellow at King Abdullah University of Science and Technology (KAUST), Kingdom of Saudi Arabia from March 2018-June 2019. Currently, he is working as postdoctoral researcher at the Research Institute of Industrial Science at Hanyang university, Seoul, South Korea since September 2019. His research interest includes core-shell NPs, metal-organic frameworks (MOFs), 1D nanostructures and room temperature gas sensors.

Ali Mirzaei received his Ph.D. degree in Materials Science and Engineering from Shiraz University in 2016. He was a visiting student at Messina University, Italy, in 2015 and from 2016–2018, he was accepted as postdoctoral fellow at Hanyang University in Seoul. He has author or co-author of more than 110 peer-review papers, including 15 review papers. Currently, he is assistant professor of materials science and engineering at Shiraz university of technology, Iran. He is interested in the synthesis and characterization of nanocomposites for gas sensing applications.

Hyoun Woo Kim joined the Division of Materials Science and Engineering at Hanyang University as a full professor in 2011, after 10 years working at Inha University. He received his B.S. and M. S. degrees from Seoul National University and his Ph.D. degree from Massachusetts Institute of Technology (MIT) in electronic materials in 1986, 1988, and 1994, respectively. He was a senior researcher in the Samsung Electronics Co., from 1994 to 2000. He was a visiting professor at the Department of Chemistry of the Michigan State University, in 2009. His research interests include the one-dimensional nanostructures, nanosheets, and gas sensors.

Sang Sub Kim joined the Department of Materials Science and Engineering, Inha University, in 2007 as a full professor. He received his B.S. degree from Seoul National University and his M.S and Ph.D. degrees from POSTECH in Material Science and Engineering in 1987, 1990, and 1994, respectively. He was a visiting researcher at NIMS, Japan, for 2 years each in 1995 and 2000. In 2006, he was a visiting professor at University of Alberta, Canada. In 2010, he served as a cooperative professor at Nagaoka University of Technology, Japan. His research interests include the one-dimensional nanostructures, nanosheets, and gas sensors.

Tae Whan Kim received his Ph.D. from the Department of Physics, State University of New York at Buffalo, in 1989. He is the HYU Distinguished Professor in the Department of Electronic Engineering, Hanyang University. His current research interests include the fabrication of memristive devices, organic light-emitting devices, nanogenerators, and sensors.